Dynamics of p53 in single cells: physiologically based ODE and reaction-diffusion PDE models

Jan Elias, Luna Dimitrio, Jean Clairambault, Roberto Natalini

Dynamics of p53 in single cells: physiologically based ODE and reaction–diffusion PDE models

Ján Eliaš

UPMC, Laboratoire Jacques-Louis Lions, 4 Place Jussieu, F-75005 Paris, France & INRIA Paris-Rocquencourt, MAMBA project-team, Paris and Rocquencourt, France

E-mail: jan.elias@inria.fr

Luna Dimitrio

On leave from UPMC, Laboratoire Jacques-Louis Lions, 4 Place Jussieu, F-75005 Paris, France & on leave from INRIA Paris-Rocquencourt, MAMBA project-team, Paris and Rocquencourt, France

Jean Clairambault

UPMC, Laboratoire Jacques-Louis Lions, 4 Place Jussieu, F-75005 Paris, France & INRIA Paris-Rocquencourt, MAMBA project-team, Paris and Rocquencourt, France

Roberto Natalini

Istituto per le Applicazioni del Calcolo Mauro Picone, CNR, Rome, Italy & Dipartimento di Matematica, Università di Roma Tor Vergata, Rome, Italy

Abstract. The intracellular signalling network of the p53 protein plays important roles in the genome protection and the control of cell cycle phase transitions. Recently observed oscillatory behaviour in single cells under stress conditions inspires several research groups in simulating and studying the dynamics of the protein with the perspective of a proper understanding of physiological meanings of the oscillations. We propose compartmental ODE and PDE models of p53 activation and regulation in single cells following DNA damage and we show that the p53 oscillations can be retrieved by plainly involving p53–Mdm2 and ATM–p53–Wip1 negative feedbacks, which are sufficient for oscillations experimentally, with no further need to introduce any delays into the protein responses and without considering additional positive feedback.

Keywords: Protein signalling, p53 network, oscillations, ODE, PDE, compartmentalisation.

Submitted to: *Phys. Biol.*

1. Introduction

The protein p53 is a transcription factor protein which controls, for example, transitions from G1 to S and from G2 to mitosis cell cycle phases during a tissue development and subsequent tissue regeneration relying on the divisions of cells at mitosis. The p53 protein can respond to abnormal developmental pathways triggered by oncogene or tumour suppressor gene mutations, thus preventing the cell from turning it into a malignant cell (for this reason the p53 gene has been called a "tumour suppressor" gene) [32]. It is also activated whenever the cell DNA is exposed to various stress conditions such as ionising γ-radiation, UV or various drugs in chemotherapies causing DNA damage and also by agents which do not cause DNA damage, for example, hypoxia, starvation, heat and cold, *etc.*, [30]. As a response to these stresses, p53 transcriptionally activates a bench of pro-arrest and pro-apoptotic proteins leading either to cell cycle arrest (and thus it enables repair processes to fix the DNA damage), senescence or apoptosis [55], apparently, with no ability of p53 to preferentially activate pro-arrest target genes rather than pro-apoptotic genes due to the higher/lower affinity of p53 for these genes [28].

Although mutations of the p53 gene primarily do not cause cancer, inactivation of its transcriptional activity, mostly due to missense mutations located in the DNA-binding domain [25], can lead to failures in the prevention of unnatural growth whenever some other mutations of genes causing uncontrolled growth occur. Notably, p53 mutations are common in human cancers (they occur in about 50% of mammalian cancer cells), and are frequently associated with aggressive disease courses and drug resistance, for example, in cases of patients with AML at diagnosis (with mutations in the p53 gene of 10%-15% initially) [54]. Interestingly, patients with rare p53 gene germ line mutations known as Li-Fraumeni syndrome have an approximately 90% lifetime risk of developing cancer (50% before the age of 40 years) [34].

The protein p53 is a well studied protein due to its role in the protection of the genome; furthermore, because p53 can elicit life or death decisions in cells, it has recently become a therapeutic target in cancer treatment. Therapeutic effort in p53-aimed treatments focuses mainly on either substitution of the p53 lost functionality and destabilisation of oncogenic p53 mutants, or restoration of p53 function by targeting upstream proteins in the p53 signalling pathway, in particular the negative regulator Mdm2 which, in some cancer cells, is over-expressed and thus suppresses the p53 functionality, see [25, 30] and citations therein.

With the perspective of future implications and predictions of possible intramolecular drug effects on p53 (or proteins in its signalling pathways) we propose physiologically based mathematical models of p53 activation and activity toward its upstream targets Mdm2 and Wip1 in response to DNA damage, assuming in this study p53 to have full functional capability to act as a physiological transcription factor.

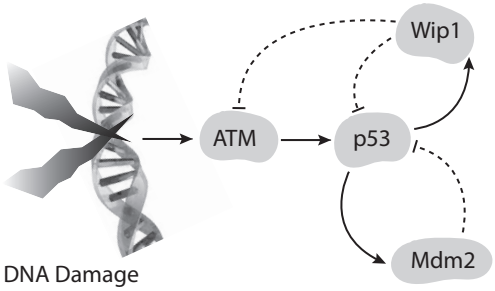

Figure 1: The studied p53 dynamics: in response to DNA damage, ATM is activated and phosphorylates p53, which results in inhibition of the p53–Mdm2 compound formation; p53 accumulates in the nucleus and acts as a transcription factor for Mdm2 and Wip1; Wip1 dephosphorylates ATM and p53 keeping them inactive and enabling Mdm2 to bind p53 again, Mdm2 initiates ubiqitinatation of p53, its nuclear export and degradation.

2. Rationale for a new p53 modelling – differences from existing models relying on single cell measurements

In the very simplified p53 dynamics represented here the ATM protein is firstly activated in response to DNA damage [2]. Activated ATM then phosphorylates p53 on serine 15 which disrupts binding to its main regulator, the E3 ligase Mdm2, a transcription target for p53. The regulation of p53 by Mdm2 is predominantly achieved through (multiple-)ubiquitination, followed by nuclear export of p53 and subsequent degradation [55]. Such regulation by Mdm2 is possible due to previous p53 deactivation, i.e., serine 15 dephosphorylation by the phosphatase Wip1, which also dephosphorylates ATM, rendering the proteins inactive [42, 43].

The most pioneering works revealing experimentally p53 oscillations in single cells have been performed by the research group at Galit Lahav's Laboratory, see for example [4, 20, 29, 35]. In particular, it has been shown that the negative feedbacks p53–Mdm2 and ATM–p53–Wip1 are essential to maintain sustained oscillations in the p53 concentration [4], observed in the majority of cells following exposure of γ-radiation doses and other stress agents [29]. The p53–Mdm2 negative feedback, however, primarily functions to gain homeostasis (keeping the concentration of p53 at low levels) rather than oscillations [47], and since ATM–p53–Wip1 is also a negative feedback, a time delay has to be imposed into these negative feedbacks by other means to reproduce sustained oscillations. Specific mathematical models thus either directly impose delays onto the equations (and thus use delayed differential equations, DDEs) or involve intercompartmental transport of species, often coupled by a positive feedback (primarily via ODEs).

Note, that there are 7 known negative feedbacks regulating p53 (6 of them between p53 and Mdm2, and other proteins) and at least 7 positive feedbacks (PTEN, p14/19 ARF, Rb, Dapk1, c-Ha-Ras, DDR1, Rorα) [22, 27]. Models in [8, 27, 52] simulate the p53 intracellular dynamics by combining the p53–Mdm2 negative feedback with a positive

feedback loop, often with the p53–PTEN–PIP3–Akt positive feedback. Compartmental models in [13, 36, 38, 49] consider the negative feedback p53–Mdm2 alone to yield p53 oscillations either by DDEs or by explicitly distinguishing in processes related to p53 pathways between the nucleus and the cytoplasm (transcription of genes in the nucleus, translation in the cytoplasm). The ODE model in [53] couples the p53-Mdm2 and ATM-p53-Wip1 negative feedback loops with the molecular transport of Mdm2 between the nucleus and the cytoplasm (controlled by the Akt-dependent phosphorylation) to produce sustained oscillations. A mathematical model developed in [4] also uses these two negative feedbacks to simulate the p53 dynamics *in silico*, although with general variables: *a signal* (including ATM) that initiates p53 signalling and *an inhibitor* (including Wip1) that inhibits the p53-directed signalling activity, by using DDEs to impose delays into the protein responses. However, DDE models may generate artificial rhythms in systems, which do not appear naturally, see [27] and references therein, so that the biological significance of the introduced delays in modelling the protein signalling is most often far from obvious in those DDE models. Avoiding DDEs, the authors in [27] convert the DDE system [4] into a system of ODEs. However, they still need to involve a positive feedback (they chose a recently observed positive feedback involving Rorα) to obtain oscillations.

We have shown in [14] that whenever classical Michaelis–Menten kinetics (see, for example, [26] Chapter 1) is used to mathematically describe protein reactions in a modelling setting where compartmental localisation of cellular events nor any positive feedback is considered, the two negative feedbacks do not produce oscillations (and eventually lead to p53 homeostasis). Instead of taking any of the observed positive feedbacks (although different positive feedbacks may play a prime role in different phases of the p53 signalling [22, 55]; however, none of them has been reported as necessary for oscillations in [4]), it is sufficient to distinguish between cellular events occurring either in the nucleus or in the cytoplasm, that represent actual processes occurring in the cell, to obtain sustainedly oscillating p53 concentration that is compatible with experimental observations.

Compartmental distribution of cellular events between the nucleus (e.g., gene transcription, p53 activation by ATM and its deactivation by Wip1) and the cytoplasm (e.g., mRNA translation into proteins, p53 degradation), however, suggests to involve spatial variables [13]. Thus, based on our compartmental ODE model [14], we propose to model the ATM/p53/Mdm2/Wip1 protein dynamics as a reaction–diffusion problem with transmission between nucleus and cytoplasm, and we numerically solve it in 2D and 3D, subsequently comparing the results of the PDE model with those given by the ODE model [14], and with biological observations. To our best knowledge, the only spatio–temporal p53/Mdm2 models formulated by PDEs are proposed in [13, 45]; however, they contain neither ATM nor Wip1 signalling.

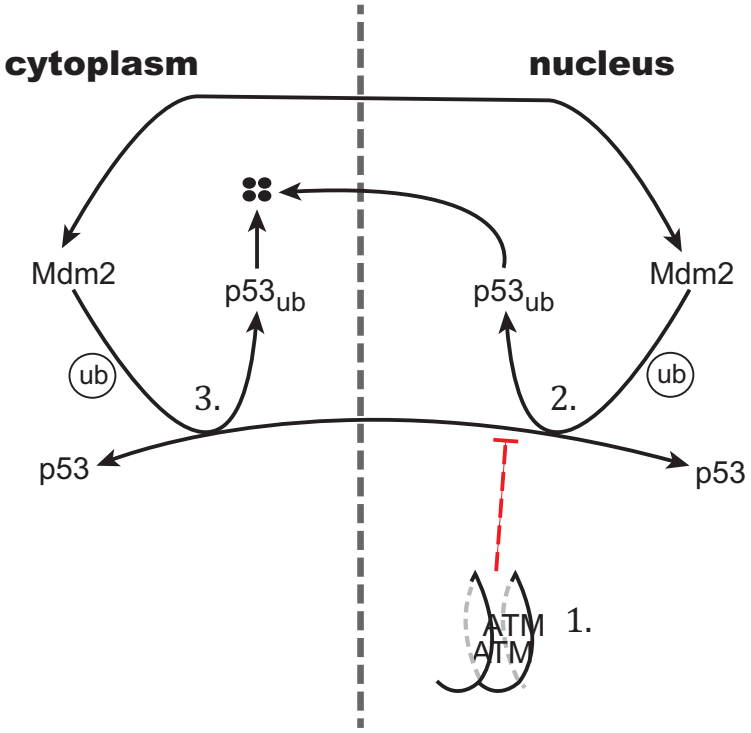

Figure 2: p53 dynamics in a normal unstressed cell: 1. The protein ATM in its inactive form is dimerised, unable to phosphorylate p53, which subsequently cannot act as a transcription factor. p53 and Mdm2 are both assumed to freely migrate between the compartments, however, Mdm2-ubiquitin dependent degradation in the nucleus, 2., and in the cytoplasm, 3., retains the concentration of p53 at low levels in the compartments. *Arrows in this sketch either indicate directions of molecule migrations or schematically show reactions in the signalling pathway.*

3. Model assumptions

In the following sections, we briefly present and discuss the cellular events under consideration. The p53 dynamics before and after exposure of a cell to a stress (e.g., DNA damage) is schematically shown on Figure 2 and on Figure 3, respectively.

3.1. p53 degradation

Regulation of p53 is dominantly achieved through the ubiquitin-dependent degradation controlled by the E3 ligase Mdm2 [30, 33]. Once p53 is sufficiently ubiquitinated, such labeled p53 protein is exported to the cytoplasm and degraded by the protein-degrading machinery [47]. Mdm2 plays a crucial role in the p53 ubiquitination as it attaches the first ubiquitin to p53. The effective p53 degradation requires p53 to be polyubiquitinated with important contribution from other proteins, e.g. p300 [33]; however, for the sake of simplicity we assume that the sole ubiquitination by Mdm2 is sufficient for p53 nuclear export and degradation. In addition, we are aware of the activity of other proteins in

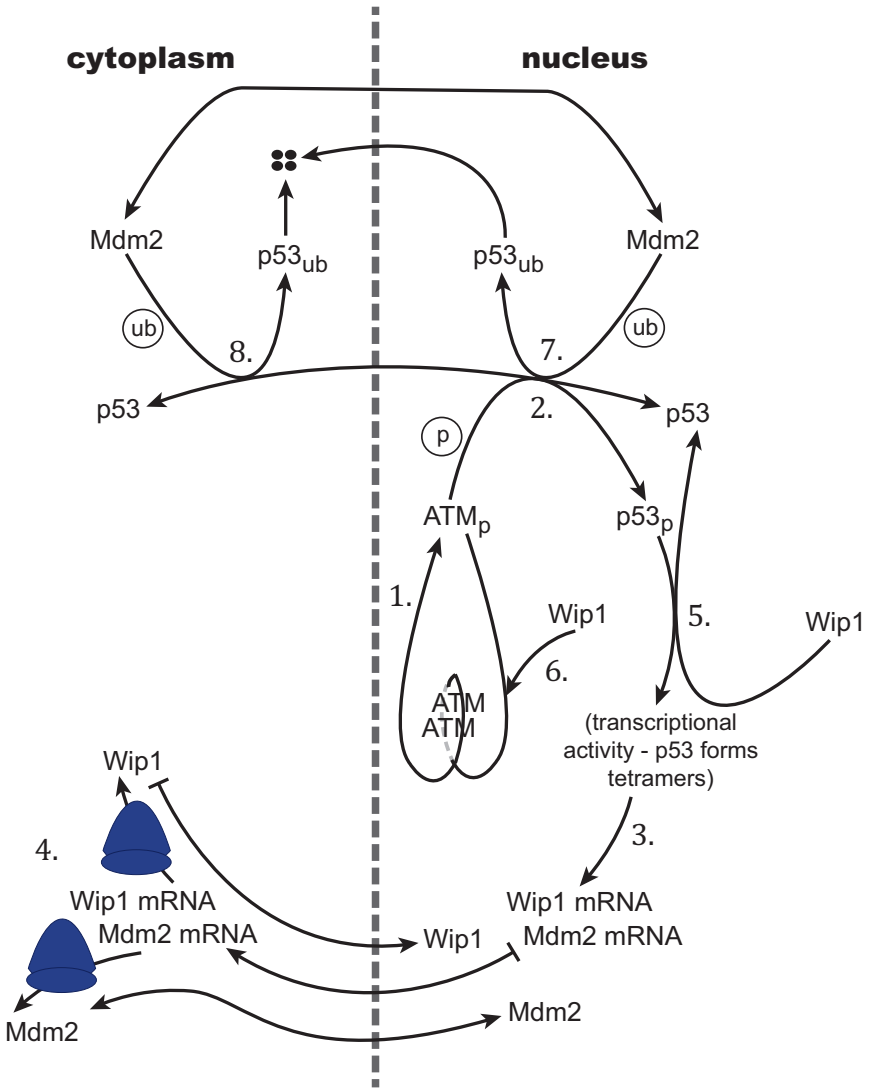

Figure 3: p53 dynamics under stress conditions: 1. ATM autophosphorylation (a consequence of the exposure to stress conditions, e.g., γ-radiation) results in ATM dimer dissociation into active monomers ATM_p, which, 2., can phosphorylate p53 (ATM_p and $p53_p$ do not leave the nucleus). 3. Phosphorylated p53 forms tetramers which bind DNA and act transcriptionally for Mdm2 and Wip1. 4. The mRNAs of the proteins leave the nucleus, bind ribosomes and they are translated into proteins; Wip1 moves into the nucleus only while Mdm2 acts in both compartments. 5. Wip1 dephosphorylates $p53_p$, making it visible for Mdm2. 6. Wip1 also dephosphorylates ATM_p which dimerises with another dephosphorylated ATM molecule. Dephosphorylated p53 can freely migrate between the compartments, where, 7. and 8., it can be ubiquitinated by Mdm2 and subsequently degraded. *Arrows in this sketch either indicate directions of molecule migrations, uni- or bidirectional, T-shaped lines meaning impossible nucleocytoplasmic transport in the T-end direction, or schematically show reactions in the signalling pathways.*

cells that can deubiquitinate p53, such as the hydrolase Hausp, which contribute to p53 stabilisation [55]. Here, p53 degradation is represented mainly by "the single-attached-ubiquitin Mdm2-dependent loss" of p53 in both nucleus and cytoplasm, but we also add a natural Mdm2-independent degradation term for cytoplasmic p53.

3.2. p53 production

Abundance of the p53 protein is mainly determined by its degradation rather than by its production [47]. Thus, we include a basal production rate for the p53 protein as the only source for p53. The basal production rate is a constant and, similarly to [45], we assume that the basal production rate is active only in a ring-shaped region of the cytoplasm (an annulus) separated from the nucleus by the endoplasmic reticulum (ER), since proteins produced in the ER very likely do not enter the nucleus [1, 45]; this ring-shaped area will be specified later (see Section 4.7).

3.3. p53 transcriptional activation and activity

The protein p53 can be activated in at least three independent ways in response to different stresses [30, 47]. In highly specific situations, different stress conditions can lead to different p53 post-translational modifications and thus to different responses to the stresses [55]. The occurrence of DNA double strand breaks (DSBs), caused by radiation doses or cytotoxic drugs in chemotherapy, initiates the activation of ATM, a sensor of DNA DSBs [16] (see below for more details). The activated ATM protein phosphorylates p53, which results into the dissociation of the p53-Mdm2 complex and accumulation of p53 in the nucleus, since Mdm2 is disabled from further p53 ubiquitination and thus phosporylated $p53_p$ cannot be exported from the nucleus and degraded. Note also that unlike $p53_p$, p53 can freely migrate between the compartments.

The phosphorylated protein p53 preferentially forms tetramers, binds DNA and transcriptionally acts as a tetramer [19, 25, 50]. Hence, we model transcription of the genes by using Hill functions with coefficient 4, since we adopt a generally accepted principle according to which the Hill coefficient is equal to the number of binding sites of a transcription factor [50] .

3.4. The expression of Mdm2 and Wip1 genes

Although transcription of Mdm2 and Wip1 genes into mRNA is mainly controlled by the active tetrameric $p53_p$ compound, we consider also a constant basal p53-independent production rate. The mRNAs of Mdm2 and Wip1 then move from the transcription sites in the nucleus to the cytoplasm (but not back) and bind ribosomes. We assume that translation of mRNAs into proteins occurs in the cytoplasm only, but also and again by following [1, 45], for the proteins considered in this model, only outside of the ER. Translation is modelled as a linear contribution to the overall protein concentrations. Importantly, in our models we consider equations for the free mRNA present in the

cell. Thus the mRNA bound to ribosomes is counted as loss from the total free mRNA. Degradation terms for mRNAs are included.

3.5. The activity of Mdm2 and Wip1 proteins

The protein Mdm2 can freely migrate between the compartments and it also can ubiquitinate unphosphorylated p53 in both compartments. The phosphatase Wip1 is assumed to move from the cytoplasm to the nucleus only since it is predominantly found to be the nuclear protein [17]. Wip1 then dephosphorylates and thus inactivates both p53 and ATM, enabling Mdm2 to bind p53 and disabling ATM from phosphorylating p53. The only assumed way by which Mdm2 and Wip1 are regulated is through degradation of the proteins and their mRNAs.

3.6. ATM activation in response to DSBs

ATM in inactive state forms dominantly dimeric complexes rendering ATM stable (non-changing) in concentration and unable to phosphorylate upstream targets [2]. In response to DSBs, *in vivo* ATM dimers sense the DNA damage, very likely due to changes in chromatin structure and a cascade of subsequent phosphorylation events, followed by ATM dimer dissociation into active monomers occurring at distance from DNA DSBs [2]. *In vitro*, the Mre11/Rad50/Nbs1 protein complex (MRN) binds DNA DSB sites, unwinds DNA ends, recruits ATM dimers to these DNA sites where they finally dissociate into active monomers and phosphorylate upstream targets, possibly, with a fraction of ATM monomers released back into the nucleus [31]. Whether ATM is activated adjacent to or at a distance from the DNA, its activation is observed to be very fast, and we represent ATM monomerisation and activation as an enzymatic reaction initiated by an unknown signal E, assumed to be a hypothetical molecule, hereafter expressed in μM, corresponding to the importance of the DNA damage (produced either by changes in the chromatin or the MRN complex).

Activated ATM_p is considered to be a strictly nuclear protein, although a fraction of ATM molecules is found in the cytoplasm however with no kinase activity on p53 following DNA damage [51]. Thus, we also assume that p53 phosphorylation by ATM can occur only in the nucleus. Due to the big weight of ATM ($\sim$370 kDa) we do not assume inter-compartmental migration of ATM, ATM degradation and production of new ATM molecules. Instead, we hypothesise that ATM switches between active monomeric and inactive dimeric states, remaining thus in overall constant concentration, an assumption that is supported by experiments reported in [2].

3.7. Final assumptions

In addition to the aforementioned assumptions, we assume in the ODE version of the model that the concentrations of all the proteins and of the mRNAs are homogenous in the compartments (this will not be the case anymore in its PDE version where diffusion

is present, see below). Ubiquitination and phosphorylation are modelled classically as kinetic reactions by the law of mass action and the quasi-steady-state approximation ([26], Chapter 1). Whenever possible, the kinetic parameters are collected from literature, others are chosen so as to obtain oscillatory responses to DNA damage.

4. Modelling p53 dynamics: physiological ODE and reaction-diffusion PDE models

4.1. Mathematical formalism and notation

A simplified cell model consists of two compartments, the nucleus Ω_1 and the cytoplasm Ω_2 with the nuclear membrane Γ_1 and the cellular membrane Γ_2, as it is schematically shown on Figure 4.

For simplicity, let us denote the concentrations of proteins in their nuclear and cytoplasmic states (distinguished by the superscripts (n) and (c), respectively) as follows

$$\begin{aligned} &u_0 = [p53]^{(n)}, u_1 = [Mdm2]^{(n)}, u_2 = [Mdm2_{mRNA}]^{(n)}, u_3 = [p53_p]^{(n)}, \\ &u_4 = [ATM_p]^{(n)}, u_5 = [Wip1]^{(n)}, u_6 = [Wip1_{mRNA}]^{(n)}, \\ &v_0 = [p53]^{(c)}, v_1 = [Mdm2]^{(c)}, v_2 = [Mdm2_{mRNA}]^{(c)}, v_3 = [p53_p]^{(c)}, \\ &v_4 = [ATM_p]^{(c)}, v_5 = [Wip1]^{(c)}, v_6 = [Wip1_{mRNA}]^{(c)} \end{aligned} \tag{1}$$

where $u_i = u_i(t, \mathbf{x})$, $u_i : [0, T] \times \Omega_1 \to \mathbb{R}$ $\forall i = 0, 1, \ldots, 6$, and $v_j = v_j(t, \mathbf{x})$, $v_j : [0, T] \times \Omega_2 \to \mathbb{R}$ $\forall j = 0, 1, \ldots, 6$; $\Omega_1 \subset \mathbb{R}^d$, $\Omega_2 \subset \mathbb{R}^d$, $d = 2, 3$, are open and bounded domains with smooth boundaries. Note that in the ODE case, the concentrations are functions of time only, not of a spatial variable $\mathbf{x}$, which plays an essential part in the PDE model.

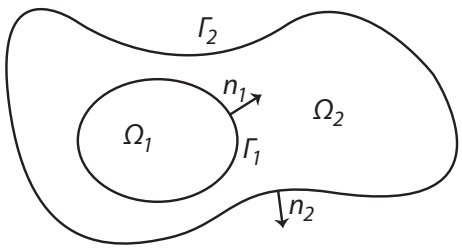

Figure 4: A schematic cell representation: a typical cell represented here consists of the nucleus Ω_1, the cytoplasm Ω_2, the nuclear membrane Γ_1 and the cell membrane Γ_2; $\mathbf{n}_1$ and $\mathbf{n}_2$ are the unit normal vectors oriented outward from the nucleus and from the outer cell membrane, respectively.

In unstressed cells the levels of ATM and p53 are very low, even not detectable in some cells, thus initially we set $u_i(0, \mathbf{x}) = u_i^0 = 0$ and $v_j(0, \mathbf{x}) = v_j^0 = 0$ $\forall i, j = 0, 1, \ldots, 6$ (even for Mdm2 which can be presented in cells keeping p53 at low concentrations). Reaction terms of the considered reactions, transmission conditions through Γ_1 and boundary conditions on Γ_2 are specified in the following sections. Note that, although

Ω_1	Ω_2
$\frac{\mathrm{d}u_0}{\mathrm{d}t} = k_{dph1}u_5\frac{u_3}{K_{dph1}+u_3} - k_1u_1\frac{u_0}{K_1+u_0} - k_{ph1}u_4\frac{u_0}{K_{ph1}+u_0}$ $-p_0V_r(u_0-v_0)$	$\frac{\mathrm{d}v_0}{\mathrm{d}t} = k_S - k_1v_1\frac{v_0}{K_1+v_0} - p_0(v_0-u_0)$ $-\delta_0v_0$
$\frac{\mathrm{d}u_1}{\mathrm{d}t} = -p_1V_r(u_1-v_1) - \delta_1u_1$	$\frac{\mathrm{d}v_1}{\mathrm{d}t} = k_{tm}v_2 - p_1(v_1-u_1) - \delta_1v_1$
$\frac{\mathrm{d}u_2}{\mathrm{d}t} = k_{Sm} + k_{S_{pm}}\frac{u_3^4}{K_{S_{pm}}^4+u_3^4} - p_2V_ru_2 - \delta_2u_2$	$\frac{\mathrm{d}v_2}{\mathrm{d}t} = p_2u_2 - k_{tm}v_2 - \delta_2v_2$
$\frac{\mathrm{d}u_3}{\mathrm{d}t} = k_{ph1}u_4\frac{u_0}{K_{ph1}+u_0} - k_{dph1}u_5\frac{u_3}{K_{dph1}+u_3}$	$\frac{\mathrm{d}v_3}{\mathrm{d}t} = 0$
$\frac{\mathrm{d}u_4}{\mathrm{d}t} = k_{ph2}E\frac{ATM_{TOT}-u_4}{K_{ph2}+\frac{1}{2}(ATM_{TOT}-u_4)} - 2k_{dph2}u_5\frac{u_4^2}{K_{dph2}+u_4^2}$	$\frac{\mathrm{d}v_4}{\mathrm{d}t} = 0$
$\frac{\mathrm{d}u_5}{\mathrm{d}t} = p_5V_rv_5 - \delta_5u_5$	$\frac{\mathrm{d}v_5}{\mathrm{d}t} = k_{tw}v_6 - p_5v_5 - \delta_5v_5$
$\frac{\mathrm{d}u_6}{\mathrm{d}t} = k_{Sw} + k_{S_{pw}}\frac{u_3^4}{K_{S_{pw}}^4+u_3^4} - p_6V_ru_6 - \delta_6u_6$	$\frac{\mathrm{d}v_6}{\mathrm{d}t} = p_6u_6 - k_{tw}v_6 - \delta_6v_6$

Table 1: The ODE system of equations.

based on our assumptions we have $v_3 = 0$ and $v_4 = 0$, we will involve these species in the equations to make overall notation easier to follow.

4.2. ODE model

The physiological ODE model for the dynamics of the p53 network is developed and examined in [14]. The model consists of the equations listed in Table 1 with the parameter set of Table 2. The transmission conditions through Γ_1 are expressed as differences of the concentrations of species in both compartments multiplied by permeability coefficients (p_k for $k = 0, 1, 2, 5$ and 6, see Table 2) and a special volume ratio $V_r = 10$ due to different velocities of reactions occurring either in the nucleus or in the cytoplasm [8].

Let us write $\mathbf{u} = [u_0, u_1, \ldots, u_6]^T$ and $\mathbf{v} = [u_0, u_1, \ldots, u_6]^T$; $\mathbf{f}(\mathbf{u}, \mathbf{v}) = [f_0, f_1, \ldots, f_6]^T(\mathbf{u}, \mathbf{v})$ and $\mathbf{g}(\mathbf{u}, \mathbf{v}) = [g_0, g_1, \ldots, g_6]^T(\mathbf{u}, \mathbf{v})$ for the reaction terms rising from the Michaelis-Menten kinetics and the transmission-like terms, i.e. the terms standing on the right-hand side of the ODE equations in Table 1. Thus, we can write the ODE equations as a coupled system

$$\frac{\mathrm{d}\mathbf{u}}{\mathrm{d}t} = \mathbf{f}(\mathbf{u}, \mathbf{v}) \quad \text{and} \quad \frac{\mathrm{d}\mathbf{v}}{\mathrm{d}t} = \mathbf{g}(\mathbf{u}, \mathbf{v}) \tag{2}$$

with the initial conditions $\mathbf{u}(0) = \mathbf{u}^0 = \mathbf{0}$ and $\mathbf{v}(0) = \mathbf{v}^0 = \mathbf{0}$.

4.3. Reaction-diffusion PDE model

Based on the ODE model (2), by adding a diffusion term in each equation we can formulate a reaction–diffusion model describing the evolution of the concentrations of proteins as functions of time and space in a cell composed of the two compartments, Figure 4. The dynamics of the proteins including directions of their migration through the membranes remains unchanged, Figure 3. The corresponding equations are summarised in Table 3, where, except for the permeability coefficients, all the

Parameter	Value [Units]	Description
k_{dph1}	78 $[min^{-1}]$	Wip1-dependent p53 dephosphorylation velocity
K_{dph1}	25 $[\mu M]$	Mich.-Men. rate of Wip1-dependent p53 dephosphorylation
k_{ph1}	3 $[min^{-1}]$	p53 phosphorylation velocity
K_{ph1}	0.1 $[\mu M]$	Mich.-Men. rate of p53 phosphorylation
k_1	10 $[min^{-1}]$	p53 ubiquitination velocity
K_1	1.01 $[\mu M]$	Mich.-Men. rate of p53 ubiquitination
p_0	0.083 $[min^{-1}]$	p53 permeability
δ_0	0.2 $[min^{-1}]$	p53 degradation rate
V_r	10 $[adim]$	Volume ratio
p_1	0.04 $[min^{-1}]$	Mdm2 permeability
δ_1	0.16 $[min^{-1}]$	Mdm2 degradation rate
k_{Sm}	0.005 $[\mu M/min]$	Basal Mdm2 mRNA transcription rate
$k_{S_{pm}}$	1 $[\mu M/min]$	Mdm2 mRNA transcription velocity
$K_{S_{pm}}$	0.1 $[\mu M]$	Mich.-Men. rate of Mdm2 mRNA transcription
p_2	0.083 $[min^{-1}]$	Mdm2 mRNA permeability
δ_2	0.0001 $[min^{-1}]$	Mdm2 mRNA degradation rate
k_{tm}	1 $[min^{-1}]$	Mdm2 translation rate
k_S	0.015 $[\mu M/min]$	Basal p53 synthesis rate
p_5	0.04 $[min^{-1}]$	Wip1 permeability
δ_5	0.2 $[min^{-1}]$	Wip1 degradation rate
k_{Sw}	0.003 $[\mu M/min]$	Basal Wip1 mRNA transcription rate
$k_{S_{pw}}$	1 $[\mu M/min]$	Wip1 mRNA transcription velocity
$K_{S_{pw}}$	0.1 $[\mu M]$	Mich.-Men. rate of Wip1 mRNA transcription
p_6	0.083 $[min^{-1}]$	Wip1 mRNA permeability
δ_6	0.001 $[min^{-1}]$	Wip1 mRNA degradation rate
k_{tw}	1 $[min^{-1}]$	Wip1 translation rate
k_{dph2}	96 $[min^{-1}]$	Wip1-dependent ATM dephosphorylation velocity
K_{dph2}	26 $[\mu M]$	Mich.-Men. rate of Wip1-dependent ATM dephosphorylation
k_{ph2}	1 $[min^{-1}]$	ATM phosphorylation velocity
K_{ph2}	0.1 $[\mu M]$	Mich.-Men. rate of ATM phosphorylation
E	0.1 $[\mu M]$	Concentration of "the damage signal"
ATM_{TOT}	1.3 $[\mu M]$	Total ATM concentration

Table 2: Parameter values for the p53 dynamics.

other parameters are chosen from Table 2. New permeability (translocation) coefficients changed with respect to the spatial settings, together with new diffusion coefficients are in Table 5. Zero initial conditions are still assumed.

The reaction–diffusion model for the nuclear and cytoplasmic concentrations $\mathbf{u}(t,\mathbf{x}) = [u_0,\ldots,u_6]^T(t,\mathbf{x})$ and $\mathbf{v}(t,\mathbf{x}) = [v_0,\ldots,v_6]^T(t,\mathbf{x})$, respectively, can be written (in the vector form) by

$$\frac{\partial \mathbf{u}}{\partial t} - div(D\nabla \mathbf{u}) = \mathbf{r}_{\mathbf{\Omega_1}}(\mathbf{u}) \quad \text{on} \quad (0,T)\times\Omega_1, \tag{3}$$

and

$$\frac{\partial \mathbf{v}}{\partial t} - div(D\nabla \mathbf{v}) = \mathbf{r}_{\mathbf{\Omega_2}}(\mathbf{v}) \quad \text{on} \quad (0,T)\times\Omega_2, \tag{4}$$

Ω_1	Ω_2
$\frac{\partial u_0}{\partial t} = D_0\Delta u_0 + k_{dph1}u_5\frac{u_3}{K_{dph1}+u_3} - k_1u_1\frac{u_0}{K_1+u_0}$ $-k_{ph1}u_4\frac{u_0}{K_{ph1}+u_0}$	$\frac{\partial v_0}{\partial t} = D_0\Delta v_0 + k_S\chi_C - k_1v_1\frac{v_0}{K_1+v_0} - \delta_0 v_0$
$\frac{\partial u_1}{\partial t} = D_1\Delta u_1 - \delta_1 u_1$	$\frac{\partial v_1}{\partial t} = D_1\Delta v_1 + k_{tm}v_2\chi_{CD} - \delta_1 v_1$
$\frac{\partial u_2}{\partial t} = D_2\Delta u_2 + k_{Sm} + k_{S_{pm}}\frac{u_3^4}{K_{S_{pm}}^4+u_3^4} - \delta_2 u_2$	$\frac{\partial v_2}{\partial t} = D_2\Delta v_2 - k_{tm}v_2\chi_{CD} - \delta_2 v_2$
$\frac{\partial u_3}{\partial t} = D_3\Delta u_3 + k_{ph1}u_4\frac{u_0}{K_{ph1}+u_0} - k_{dph1}u_5\frac{u_3}{K_{dph1}+u_3}$	$\frac{\partial v_3}{\partial t} = 0$
$\frac{\partial u_4}{\partial t} = D_4\Delta u_4 + k_{ph2}E\frac{ATM_{TOT}-u_4}{K_{ph2}+\frac{1}{2}(ATM_{TOT}-u_4)}$ $-2k_{dph2}u_5\frac{u_4^2}{K_{dph2}+u_4^2}$	$\frac{\partial v_4}{\partial t} = 0$
$\frac{\partial u_5}{\partial t} = D_5\Delta u_5 - \delta_5 u_5$	$\frac{\partial v_5}{\partial t} = D_5\Delta v_5 + k_{tw}v_6\chi_{CD} - \delta_5 v_5$
$\frac{\partial u_6}{\partial t} = D_6\Delta u_6 + k_{Sw} + k_{S_{pw}}\frac{u_3^4}{K_{S_{pw}}^4+u_3^4} - \delta_6 u_6$	$\frac{\partial v_6}{\partial t} = D_6\Delta v_6 - k_{tw}v_6\chi_{CD} - \delta_6 v_6$

Table 3: The PDE system.

with the initial conditions $\mathbf{u}(0,\mathbf{x}) = \mathbf{u}^0 = \mathbf{0}$ and $\mathbf{v}(0,\mathbf{x}) = \mathbf{v}^0 = \mathbf{0}$ and boundary conditions on Γ_1 and Γ_2 specified in the next section. In (3) and (4), D is a diagonal matrix with the diffusion coefficients D_i, $i = 0, 1, \ldots, 6$, on the diagonal, and $\mathbf{r}_{\mathbf{\Omega_i}}$, $i = 1, 2$, store the (nonlinear) reaction terms, the same ones as in the ODE system, rising from the Michaelis-Menten kinetics. The p53 basal production rate and the terms related to the translation of the mRNAs into the proteins are multiplied by the characteristic functions χ_C and χ_{CD} defining areas of the cytoplasm where the protein production events occur. These functions are defined and illustrated on Figure 5 in Section 4.7.

4.4. Nucleocytoplasmic transmission boundary conditions: Kedem–Katchalsky boundary conditions

All the proteins under consideration have weights over 40 kDa (Table 5) so that they can use active transport only (and not passive transport) for their translocation between the two compartments. Similarly, mRNA–protein complexes (mRNPs), formed shortly after mRNA synthesis at the transcription site, released to the nucleoplasm and moving toward the nuclear membrane [46] have weights over 40 kDa (actually, mRNPs can be as big as 1600 kDa [12]). In addition, the protein in the mRNP usually assists in the mRNA export to the cytoplasm [10] (see also this reference for the detailed description of mRNP migration through the nuclear membrane). However, comparing time scales of cargo translocations occurring within a period measured in seconds, a few minutes at most [39], and intracellular protein(mRNA)-dependent events which may hold over hours (e.g. accumulation in a compartment, regulation and degradation of a chemical in a compartment as it is in the p53 signalling in single cells [20, 29]), we will not involve active transport mechanism here and thus keep the model as simple as possible. Instead, the transmission of a chemical is represented in our model by a diffusive flux through the

boundary that is proportional to the difference between the nuclear and the cytoplasmic concentrations of the chemical, i.e., we recall the so-called Kedem–Katchalsky boundary conditions (BCs) as they have been suggested in [6] and already applied in [13].

A driving force for the diffusive transport in the Kedem–Katchalsky BCs is the difference in concentrations at both sides of the membrane, which is the simplification of a more realistic driving force standing behind most of the passive transport processes — a chemical potential gradient — which depends not only on concentrations but also on pressure, temperature, electric field and other quantities. The same BCs can be derived easily from Fick's first law for stationary fluids (i.e. with no net movement, no bulk motion and no coupling effect of more cargoes transported simultaneously); for more details see the book [37], p. 8 and 46.

In particular, a contribution to the overall concentration (increase or decrease) of a chemical with the nuclear concentration u_i, for some i, throughout Γ_1 is defined by

$$-D_i \frac{\partial u_i}{\partial \mathbf{n}_1} = -p_i(v_i - u_i). \tag{5}$$

where v_i is the cytoplasmic concentration of the same chemical, p_i is the permeability. Equation (5) says that the flux (LHS of (5)) is equal to the difference of the concentrations across the nuclear membrane for the direction of flow from u_i to v_i if $u_i > v_i$, and the other way round if $u_i < v_i$, which is in agreement with the assumption for the particle flow (Fick's first law) to be directed from a compartment with higher concentration of the chemical to a compartment with its smaller concentration.

Similar condition, particularly,

$$D_i \frac{\partial v_i}{\partial \mathbf{n}_1} = -p_i(u_i - v_i), \tag{6}$$

is written for the cytoplasmic concentration of the chemical, however, with the minus sign because of the orientation of the normal vector $\mathbf{n}_1$ which points outward from the nucleus Ω_1 to the cytoplasm Ω_2, see Figure 4.

The Kedem–Katchalsky BCs (5) and (6) satisfy the continuity of the flux condition on the boundary (what goes out from one compartment must come in to the second compartment),

$$D_i \frac{\partial u_i}{\partial \mathbf{n}_1} = D_i \frac{\partial v_i}{\partial \mathbf{n}_1}, \tag{7}$$

however, usually, $u_i \neq v_i$ on both sides of the nuclear membrane because of the permeability of the nuclear membrane (non-zero membrane "conductance"). In contrast, continuous translocation of species throughout the nuclear membrane modelled by the transmission conditions $u_i = v_i$ together with (7) are considered in [45] (i.e. no limits on perviousness of the membrane are taken into account in [45]).

Equations (5) and (6) are applied to the chemicals which migrate between Ω_1 and Ω_2, i.e. the proteins p53 and Mdm2. Other particular cases when a chemical translocates from one compartment to another in one direction only, e.g. Mdm2 and Wip1 mRNAs which move from the nucleus to the cytoplasm and not back, and the protein Wip1,

Chemical	nuclear changes	cytoplasmic changes
p53	$-D_0\frac{\partial u_0}{\partial \mathbf{n}_1} = -p_0(v_0 - u_0)$	$D_0\frac{\partial v_0}{\partial \mathbf{n}_1} = -p_0(u_0 - v_0)$
Mdm2	$-D_1\frac{\partial u_1}{\partial \mathbf{n}_1} = -p_1(v_1 - u_1)$	$D_1\frac{\partial v_1}{\partial \mathbf{n}_1} = -p_1(u_1 - v_1)$
Mdm2 mRNA	$-D_2\frac{\partial u_2}{\partial \mathbf{n}_1} = p_2 u_2$	$D_2\frac{\partial v_2}{\partial \mathbf{n}_1} = -p_2 u_2$
$p53_p$	$-D_3\frac{\partial u_3}{\partial \mathbf{n}_1} = 0$	$D_3\frac{\partial v_3}{\partial \mathbf{n}_1} = 0$
ATM_p	$-D_4\frac{\partial u_4}{\partial \mathbf{n}_1} = 0$	$D_4\frac{\partial v_4}{\partial \mathbf{n}_1} = 0$
Wip1	$-D_5\frac{\partial u_5}{\partial \mathbf{n}_1} = -p_5 v_5$	$D_5\frac{\partial v_5}{\partial \mathbf{n}_1} = p_5 v_5$
Wip1 mRNA	$-D_6\frac{\partial u_6}{\partial \mathbf{n}_1} = p_6 u_6$	$D_6\frac{\partial v_6}{\partial \mathbf{n}_1} = -p_6 u_6$

Table 4: The Kedem–Katchalsky transmission boundary conditions on Γ_1 with the diffusion coefficients D_i and the translocation (permeability) rates p_i, $i = 0, 1, \ldots, 6$.

that moves from the cytoplasm to the nucleus only, and, finally, the cases of ATM and phosphorylated $p53_p$, that do not leave the nucleus, are simple modifications of (5) and (6) and are listed in Table 4.

In the vector form, the Kedem–Katchalsky BC can be uniquely written by

$$-D\frac{\partial \mathbf{u}}{\partial \mathbf{n}_1} = P\mathbf{g}_{\Omega_1}(\mathbf{u}, \mathbf{v}) \quad \text{and} \quad D\frac{\partial \mathbf{v}}{\partial \mathbf{n}_1} = P\mathbf{g}_{\Omega_2}(\mathbf{u}, \mathbf{v}), \tag{8}$$

where $D = diag(D_0, \ldots, D_6)$, $P = diag(p_0, \ldots, p_6)$ are diagonal matrices with the diffusion and the permeability coefficients on the diagonals, and $\mathbf{g}_{\Omega_1} = \mathbf{g}_{\Omega_1}(\mathbf{u}, \mathbf{v})$ and $\mathbf{g}_{\Omega_2} = \mathbf{g}_{\Omega_2}(\mathbf{u}, \mathbf{v})$ collect the terms on the right hand sides of the boundary conditions as they are stated in Table 4; note that $\mathbf{g}_{\Omega_1} = -\mathbf{g}_{\Omega_2}$.

Finally, we do not assume exchange of the species between cells. Thus, we set

$$D\frac{\partial \mathbf{v}}{\partial \mathbf{n}_2} = \mathbf{0} \tag{9}$$

on the cell membrane, where $\mathbf{n}_2$ is the normal vector pointed outward from the cell membrane.

4.5. Diffusion and permeability coefficients

Recent photobleaching techniques enable to track the fusion of a protein with the green fluorescent protein (GFP) and thus measure diffusion of such fused proteins. Hinow *et al.* [23] estimate the nuclear diffusion of p53 fused with GFP in H1299 human large cell lung carcinoma cell to be $\sim$900 $\mu m^2/min$, slower than the diffusion of GFP itself ($\sim$2500 $\mu m^2/min$), very likely due to multimer formation.

We can assume that an individual p53 monomer migrates faster with higher diffusivity than the measured p53–GFP diffusivity. Hence, we will use the diffusion coefficient for p53 equal to 1000 $\mu m^2/min$ as an average whether it migrates as a monomer, or multimer (however, it cannot be exported as tetramer [44]). We are also aware of the fact that diffusion can be different in time during drug-induced DNA

Chemical	Diffusion	$[\mu m^2/min]$	Permeability	$[\mu m/min]$	Weight $[kDa]$
GFP	—	2500 [23, 24]	—	—	26.9 [23]
p53-GFP	—	900 [23, 24]	—	—	∼80 [23]
p53 (monomer)	D_0	1000 [est.]	p_0	10 [est.]	43.7
Mdm2	D_1	1000 [est.]	p_1	10 [est.]	56
Mdm2 mRNP	D_2	1.8 [5, 46]	p_2	0.36 [est.]	∼1600
$p53_p$ (monomer)	D_3	1000 [est.]	p_3	0	43.7
ATM_p (monomer)	D_4	300 [est.]	p_4	0	370 [2]
Wip1	D_5	1000 [est.]	p_5	10 [est.]	61 [17]
Wip1 mRNP	D_6	1.8 [5, 46]	p_6	0.36 [est.]	∼1600

Table 5: (Estimated) diffusion and translocation (permeability) coefficients. Since we assume that $p53_p$ and ATM_p do not leave nor enter the nucleus, which is sufficiently described by the particular BCs, the permeability coefficients p_3 and p_4 can be chosen arbitrarily.

damage. For instance, the diffusion coefficient of p53–GFP significantly reduces after the drug treatment by cisplatin and etoposide in HeLa cells: both drugs induce p53 activation and accumulation in the nucleus with diffusion 900 $\mu m^2/min$ decreased up to 200 $\mu m^2/min$ measured 16 hours after anticancer drug activity [24].

Due to the lack of experimentally measured data, we set the values of the diffusion coefficients for the other proteins by comparing their weights. We will use diffusions of $1000\,\mu m^2/min$ for Mdm2 and Wip1 (56 and 61 kDa, respectively, comparing to $43.7\,kDa$ of monomeric p53) and $300\,\mu m^2/min$ for ATM ($370kDa$). Diffusion of an avarage mRNA-protein complex vary in the range $1.2-2.4\,\mu m^2/min$ [5, 46] and we will use the reference value for the mRNP complexes equal to $1.8\,\mu m^2/min$.

Transport of the species through the nuclear membrane Γ_1 is determined by the diffusion and the permeability coefficients in (8). Due to the lack of data, we have run several simulations and tested various permeability rates for which oscillations appear, as the reference one we have chosen those listed in Table 5.

All the permeability and diffusion coefficients considered in our simulations are listed in Table 5. Note that due to the similar nuclear and cytoplasmic cytosol viscosity we will consider the same diffusion values for both compartments. Note that there are also other possibilities how to approximate diffusion coefficients of proteins, for example, by using Einstein's formula [6] which, however, requires Stokes radii of the proteins, which are often not known.

4.6. Nondimensionalisation

The ODE system (2) with the equations explicitly stated in Table 1 and with the kinetic parameters in Table 2, together with the PDE system (3) and (4) with the Kedem–Katchalsky BCs (8) explicitly listed in Tables 3, 4 and with the parameters in Tables 2 and 5 are nondimensionalised before they are solved. See [41] for more details on advantages and the necessity of nondimensionalisation.

For reference concentration α_i, $i = 0, \ldots, 6$, (measured in μM) the scaled nuclear and cytoplasmic concentrations of the species are defined by, respectively,

$$\bar{u}_i = \frac{u_i}{\alpha_i} \quad \text{and} \quad \bar{v}_i = \frac{v_i}{\alpha_i}. \tag{10}$$

By setting

$$\bar{t} = \frac{t}{\tau}, \, \bar{x}_j = \frac{x_j}{L}, \, j = 1, \ldots, d \quad \text{with} \quad L = 10\mu m \tag{11}$$

and

$$\begin{aligned}
&\bar{k}_{dph1} = \tau k_{dph1}(\alpha_5/\alpha_0), \bar{K}_{dph1} = K_{dph1}/\alpha_3, \bar{k}_{ph1} = \tau k_{ph1}(\alpha_4/\alpha_0),\\
&\bar{K}_{ph1} = K_{ph1}/\alpha_0, \bar{k}_1 = \tau k_1(\alpha_1/\alpha_0), \bar{K}_1 = K_1/\alpha_0,\\
&\bar{\delta}_0 = \tau\delta_0, \bar{\delta}_1 = \tau\delta_1, \bar{\delta}_2 = \tau\delta_2, \bar{\delta}_5 = \tau\delta_5, \bar{\delta}_6 = \tau\delta_6,\\
&\bar{k}_{Sm} = \tau k_{Sm}/\alpha_2, \bar{k}_{S_{pm}} = \tau k_{S_{pm}}/\alpha_2, \bar{K}_{S_{pm}} = K_{S_{pm}}/\alpha_3,\\
&\bar{k}_{Sw} = \tau k_{Sw}/\alpha_6, \bar{k}_{S_{pw}} = \tau k_{S_{pw}}/\alpha_6, \bar{K}_{S_{pw}} = K_{S_{pw}}/\alpha_3,\\
&\bar{k}_{dph2} = \tau k_{dph2}(\alpha_5/\alpha_4), \bar{K}_{dph2} = K_{dph2}/\alpha_4^2, \bar{k}_{ph2} = \tau k_{ph2}, \bar{K}_{ph2} = K_{ph2}/\alpha_4\\
&\bar{k}_S = \tau k_S/\alpha_0, \bar{k}_{tm} = \tau k_{tm}, \bar{k}_{tw} = \tau k_{tw}, \bar{E} = E/\alpha_4,\\
&\bar{p}_i = \tau p_i \text{ for ODE (resp. } \bar{p}_i = \tau p_i/L \text{ for PDE)}, \bar{D}_i = \tau D_i/L^2 \; \forall i,
\end{aligned} \tag{12}$$

we finally arrive at the systems used in our simulations. The nondimensionalised equations for the ODE and PDE models are not shown here, since they are very similar to the nonscaled equations except for the entries replaced by their nondimensionalised substitutions. With the special choice of the reference concentrations

$$\begin{aligned}
&\alpha_0 = \alpha_3 = K_{ph1} = 0.1\,\mu M, \alpha_1 = \alpha_2 = k_{Spm}/k_{ph1} = 1/3\,\mu M,\\
&\alpha_4 = 10K_{ph2} = 1\,\mu M, \alpha_5 = 1\,\mu M, \alpha_6 = k_{Spw}/k_{ph1} = 1/3\,\mu M
\end{aligned} \tag{13}$$

we can additionally eliminate some parameters so that the number of parameters in the equation for phosphorylated ATM in the nucleus ($u_4 = [ATM_p]$ in our notations) involving our main bifurcation parameter E (defined in Section 3.6) is reduced to the minimum.

4.7. Numerical Simulations of PDEs in 2 and 3 dimensions

The nondimensionalised reaction–diffusion problem derived from (3) and (4) with the zero initial conditions and the Kedem–Katchalsky BCs (8) is solved numerically in 2 and 3 dimensions on the triangulations shown on Figure 5 by *the semi-implicit Rothe method*, see, e.g., [40], implemented in the FreeFem++ solver [18]. The cell under consideration

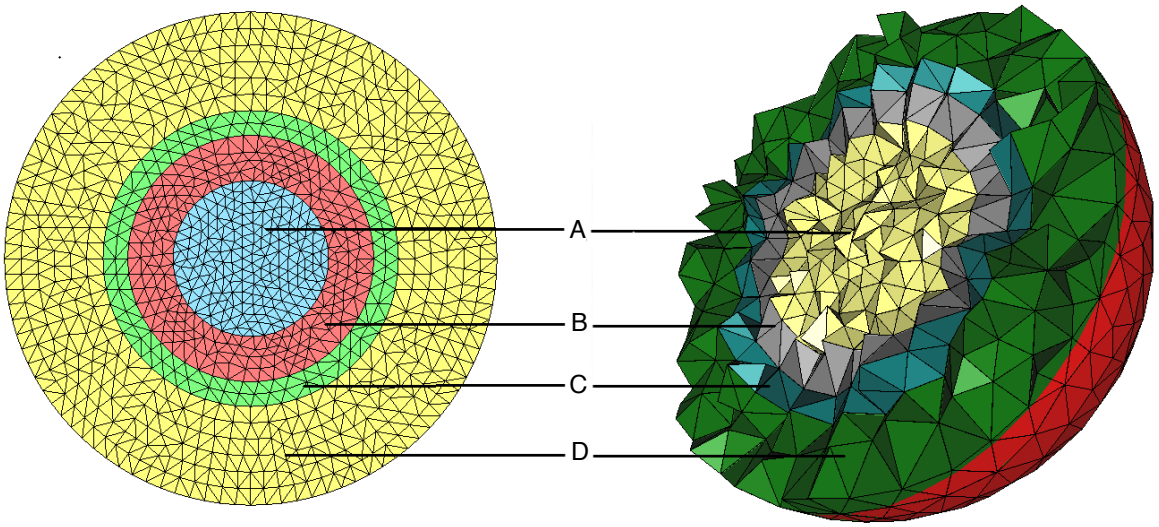

Figure 5: The 2D and 3D cell is represented by a disk and by a 3D ball, respectively, with radius $10\,\mu m$. The nucleus, A, is shown as an inner disk and an inner ball, respectively, with radius $10/\sqrt{10}\,\mu m$. The endoplasmic reticulum B, where no production of the proteins occurs, is an annulus with radii $10/\sqrt{10}\,\mu m$ and $5\,\mu m$; the ring-shaped area C, where the basal production of p53 is assumed to occur, is an annulus with radii 5 and $6\,\mu m$, respectively, and the rest of the cytoplasm, D, is an annulus with radii 6 and $10\,\mu m$. Translation of the mRNAs is supposed to occur in C+D. The 2D and 3D cell triangulations are generated by *FreeFem++* [18].

on Figure 5 has radius equal to 1 length unit, thus, by considering a scaling length $L = 10\,\mu m$, the cell model represents a real cell with size $20\,\mu m$ in diameter.

As already mentioned, the production of p53 determined by the basal production rate k_S is restricted to a narrow ring-shaped area within the cytoplasm (denoted by C on Figure 5) separated from the nucleus by the ER (denoted by B on Figure 5). Numerically, we multiply k_S by the characteristic function $\chi_C = \chi_C(\bar{\mathbf{x}})$, $\bar{\mathbf{x}} \in \Omega_2 \subset \mathbb{R}^d$, $d = 2, 3$, defined by

$$\chi_C(\bar{\mathbf{x}}) = \begin{cases} 1 & \text{for} \quad 0.5 \leq \|\bar{\mathbf{x}}\| \leq 0.6, \\ 0 & \text{otherwise.} \end{cases}$$

Similarly, translation of the Mdm2 and Wip1 mRNAs into the proteins is allowed to occur in the cytoplasm except for the endoplasmic reticulum (ER), i.e. only in the regions C and D on Figure 5. Thus, the translation terms with the rates k_{tm} and k_{tw} are multiplied by $\chi_{CD} = \chi_{CD}(\bar{\mathbf{x}})$

$$\chi_{CD}(\bar{\mathbf{x}}) = \begin{cases} 1 & \text{for} \quad 0.5 \leq \|\bar{\mathbf{x}}\| \leq 1, \\ 0 & \text{otherwise.} \end{cases}$$

Details about solving reaction-diffusion problems rising in molecular biology (as the particular one from Michaelis-Menten kinetics, possibly appearing in other problems) by the semi-implicit Rothe method is omitted and a special article dedicated to numerical

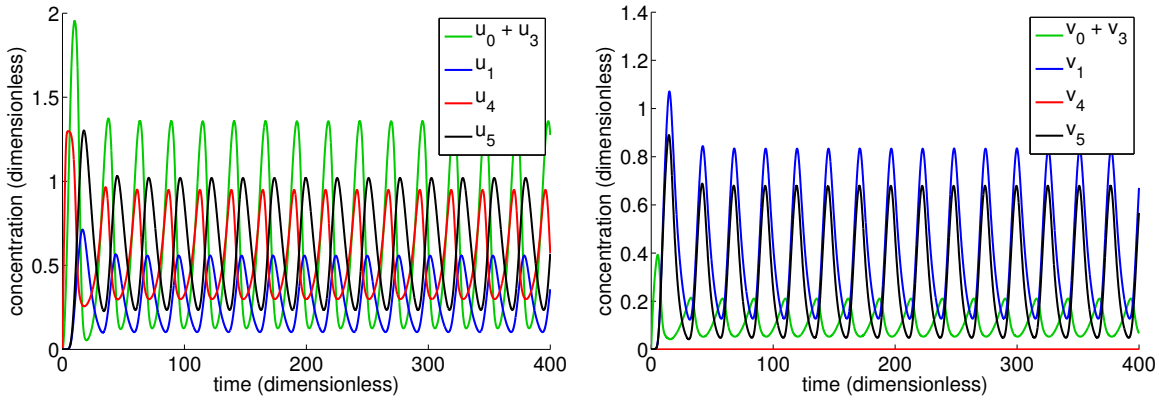

(a) (b)

Figure 6: Solution of the ODE system within 400 (dimensionless) time units for the fixed set of parameters in Table 2: nondimensionalised (a) nuclear u_i and (b) cytoplasmic v_i concentrations of $p53 + p53_p$ ($u_0 + u_3$ and $v_0 + v_3$), $Mdm2$ (u_1 and v_1), ATM_p (u_4 and v_4), and $Wip1$ (u_5 and v_5).

aspects of the modelling, giving a proof of existence and uniqueness of the solution, is in preparation [15]. Note that we have chosen the Rothe method rather than the commonly used Newton method for nonlinear PDEs because it gives accurate results computationally faster than the Newton method and, in addition, it has been found easier to implement when dealing with the systems of equations. The FreeFem++ [18] solver has been used for our simulations.

5. ODE and PDE simulations results

5.1. Oscillations of p53 in the ODE model

The ODE model (2) was assessed in [14] where, among other things, it was shown that the negative feedback loops p53–Mdm2 and ATM–p53–Wip1 with the compartmentalisation of cellular events are sufficient to produce sustained oscillations in the p53 signalling network after DNA damage (from $E = 0.1\,\mu M$). In addition, it is shown in [14] that omitting any part of the protein network or compartmentalisation leads to the convergence of the system (2) to its steady state either with a very fast rate or slowly with some damped oscillations. The plots on Figure 6 show the nondimensionalised nuclear and cytoplasmic concentrations of the proteins.

5.2. Oscillations of p53 in the PDE model

The similar evolution of the concentrations of the proteins as the one given by the ODE system shown on Figure 6 can be obtained also by solving the PDE system of equations. The semi-implicit Rothe method applied to the 2D and 3D PDE system (3) and (4) with the boundary conditions (8) and (9) indeed gives oscillatory responses

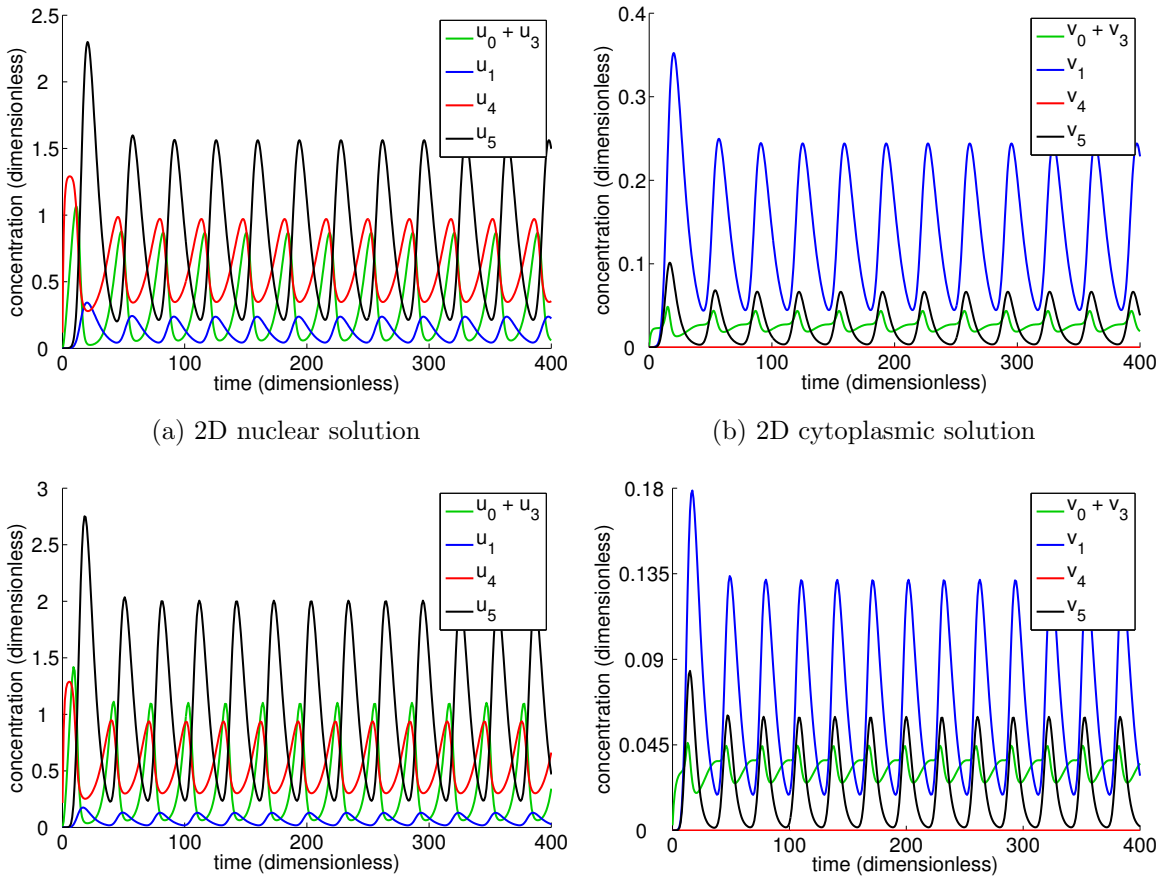

(a) 2D nuclear solution

(b) 2D cytoplasmic solution

(c) 3D nuclear solution

(d) 3D cytoplasmic solution

Figure 7: Solution of the PDE system within 400 (dimensionless) time units for the fixed set of parameters in Tables 2 and 5: nondimensionalised (a) 2D nuclear u_i, (b) 2D cytoplasmic v_i, (c) 3D nuclear u_i and (d) 3D cytoplasmic v_i concentrations of $p53+p53_p$ (u_0+u_3 and v_0+v_3), $Mdm2$ (u_1 and v_1), ATM_p (u_4 and v_4), and $Wip1$ (u_5 and v_5). The plotted concentrations are the averages through all the elements of the nuclear and cytoplasmic triangulation.

of the system to the damage signal with $E = 0.1$, see Figures 7 and 8, where, respectively, the dimensionless nuclear and cytoplasmic concentrations of the proteins and the nuclear phase planes with limit cycles are shown. Comparing Figures 6 and 7, the difference lies in the amplitudes of oscillations attained. Note that the periods of the nondimensionalised ODE and PDE solutions are also different; however, by setting $\tau_{ODE} = 14\,min$, $\tau_{2D} = 10.6\,min$ and $\tau_{3D} = 12\,min$ into $t = \tau\bar{t}$ in (11), the periods of the ODE, 2D and 3D PDE solutions, respectively, can be rescaled so that the periods become $\sim$6 hours, values at which they are experimentally observed in [4, 20].

The observed evolution of the concentrations in the PDE (and also in ODE) model follows the experimentally observed dynamics of the proteins [4, 20, 29]. In response to DNA damage ($E = 0.1$), the ATM protein is firstly activated and the phosphorylated

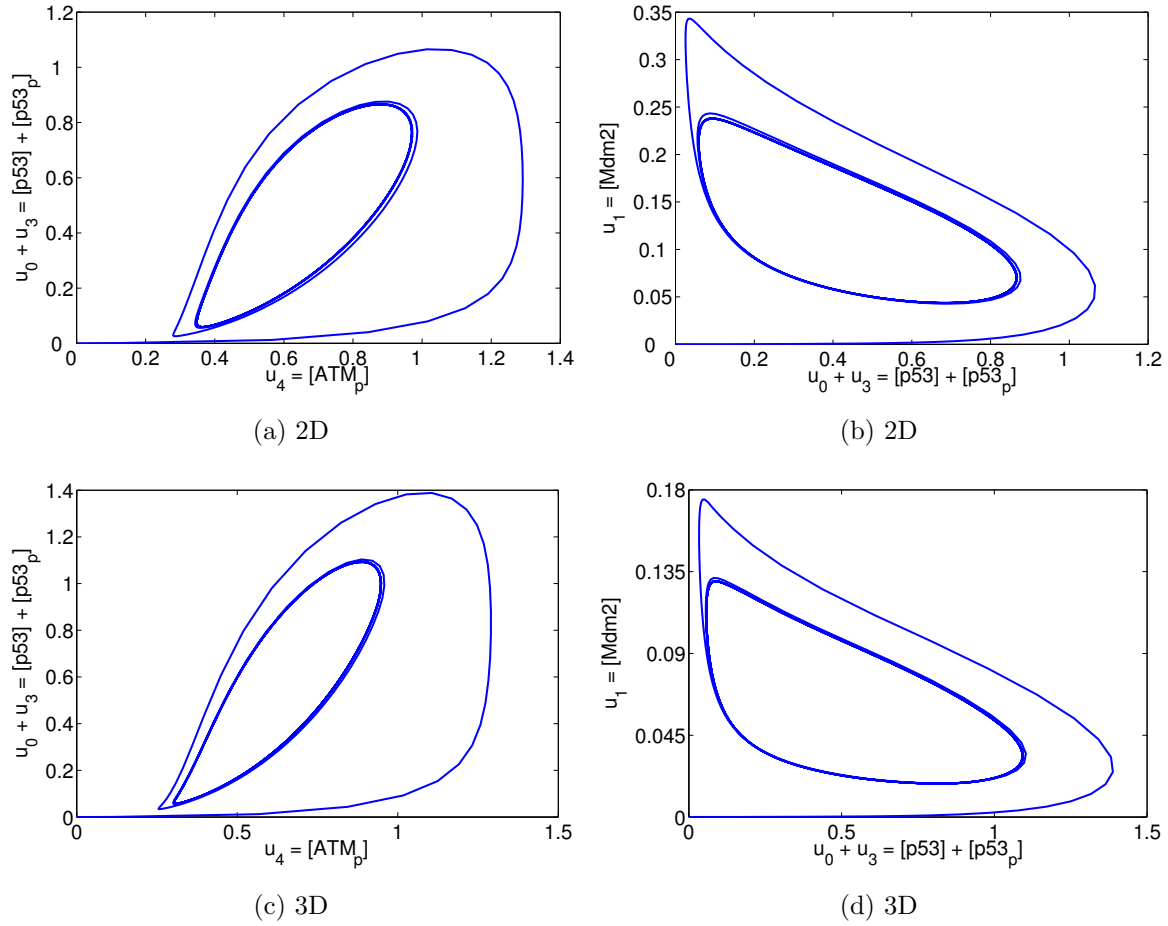

(a) 2D (b) 2D

(c) 3D (d) 3D

Figure 8: Solution of the 2D and 3D PDE system for the fixed set of parameters in Tables 2 and 5: phase portraits of dimensionless concentrations (a) and (c) $u_4 = [ATM]$ with respect to $u_0 + u_3 = [p53] + [p53_p]$ in 2D and 3D, respectively, and (b) and (d) $u_0+u_3 = [p53]+[p53_p]$ with respect to $u_1 = [Mdm2]$ in 2D and 3D, respectively. Similar stable limit cycles can be plotted for all other species.

ATM activates p53; thus the first peak in the p53 concentration pathway follows the first peak of ATM, see Figures 6 and 7 where the concentrations of the proteins are plotted. ATM is rapidly activated after DNA insult. Phosphorylated $p53_p$ accumulates in the nucleus and transcriptionally activates Mdm2 and Wip1 which move diffusively from the translation sites outside of the ER into the nucleus. The maximal levels are thus reached after the peak in the p53 concentrations. Wip1 dephosphorylates ATM which then forms dimers unable to phosphorylate p53, and also Wip1 dephsophorylates p53 making it available for Mdm2-dependent degradation. Persisting occurrence of the DNA damage (E is not assumed to change during the simulations) together with degradation of Wip1 and Mdm2 then lead to a release of the second pulse of ATM followed by a peak of p53, *etc.* It can also be seen from the figures that ATM activation is very rapid and so is the production of p53 and its activation by ATM. On the other side, Mdm2

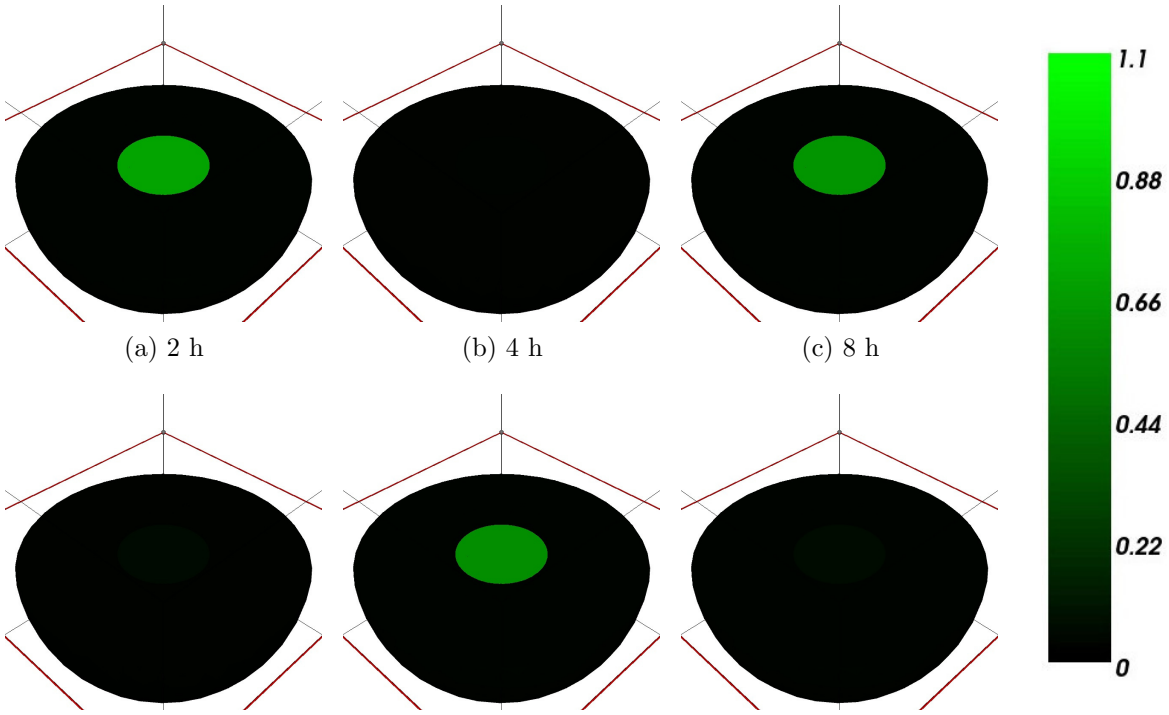

(a) 2 h (b) 4 h (c) 8 h

(d) 10 h (e) 14 h (f) 16 h

Figure 9: 3D visualisation of the solution of the PDE system for the fixed set of parameters in Tables 2 and 5: nondimensionalised concentration of $p53_p$ and $p53$. Chosen samples are captured at times (scaled by $\tau_{3D} = 12$) when p53 and Mdm2 reach peaks in their concentrations.

and Wip1 reach their peaks 2 hours (after scaling with $\tau_{2D} = 10.6\ min$ and $\tau_{3D} = 12\ min$) after the peak in the p53 concentration.

To illustrate these features, Figures 9 and 10 show samples from the spatial oscillatory evolutions of $p53_p + p53$ and Mdm2 concentrations in the 3D model of the cell captured at six time points (with time scaled by the scaling parameter τ). Recall again, that the period of the p53 oscillations can be rescaled to 6 hours, as observed, so that the first peak should appear in about 3 hours after signalling initiation; however, because of the zero initial conditions chosen this is not the case in the presented example, where the first pulse is ∼4 hours long while the second (and the others) have the period ∼6 hours.

5.3. Parameter sensitivity analysis: activation "stress" signal E

Bifurcation analysis of the ODE system with respect to the activation signal E, the main bifurcation parameter under consideration (see Section 3.6 for the introduction of E) reveals a supercritical Hopf bifurcation point $E_1 = 4.77 \times 10^{-6}$ in the equilibrium curve starting at $E = 0$ within the fixed set of parameters in Table 2. Recall that the equilibrium changes from stable to unstable by passing through the first Hopf point

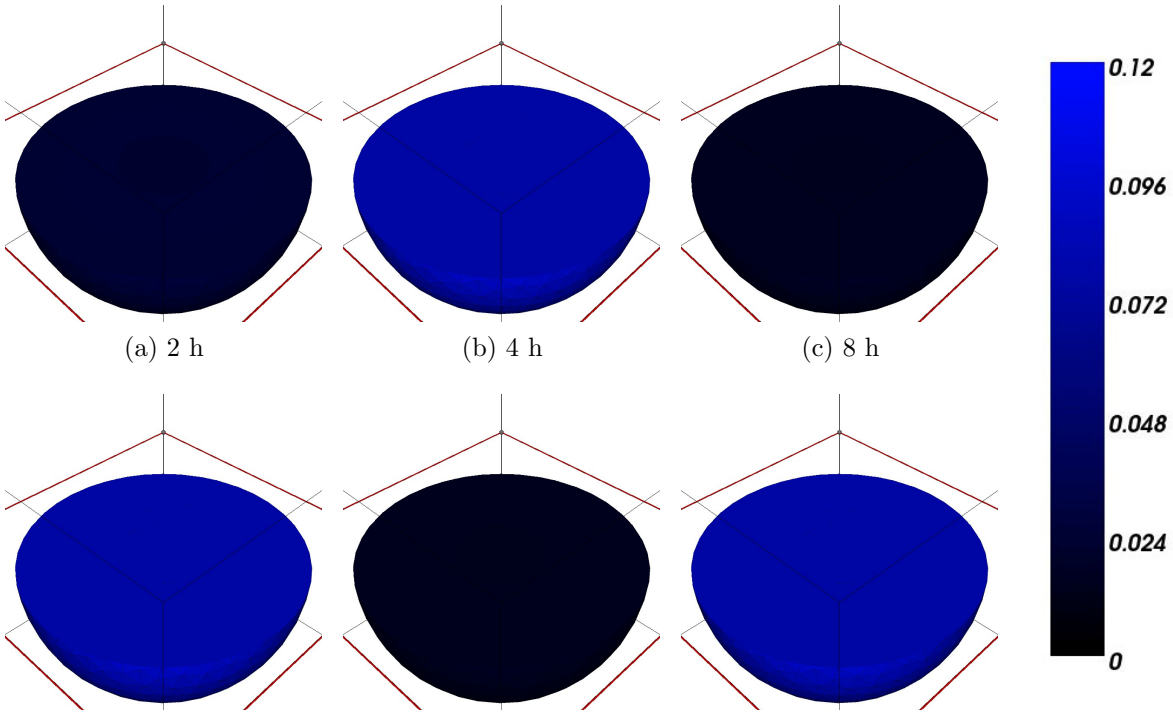

(a) 2 h (b) 4 h (c) 8 h

(d) 10 h (e) 14 h (f) 16 h

Figure 10: 3D visualisation of the solution of the PDE system for the fixed set of parameters in Tables 2 and 5: nondimensionalised concentration of $Mdm2$. Chosen samples are captured at times (scaled by $\tau_{3D} = 12$) when p53 and Mdm2 reach peaks in their in concentrations.

E_1. This means that the solution bifurcates between two qualitatively different states: convergence to a steady state for $E < E_1$, and convergence to a stable limit cycle for $E > E_1$, see Figure 11.

Similarly to the ODE system, the PDE system also exhibits two qualitatively different solutions with respect to the varying signal E; in particular, convergence of the PDE solution to a steady state is similarly changed to convergence to a stable limit cycle in crossing a bifurcation point $E_1 = 7 \times 10^{-5}$ in the 2D case and $E_1 = 4 \times 10^{-5}$ in the 3D case (with respect to the fixed set of parameters from Tables 2 and 5), Figure 12.

These significant points are very small, confirming that ATM and p53 activation is sensitive even to damage producing such a small E, [2, 3, 51], which, in turn, is able to activate ATM, and so p53, with concentrations that sustainedly oscillate in time. Furthermore, the ODE and PDE systems remain in the oscillatory regime for all $E > E_1$. Recall again in this place that the activation signal E is considered here to be a measure of the DNA damage in cells exposed to stress conditions, so that these results are in agreement with the experiments saying that the duration of p53 oscillations is independent of the damage dose [29, 35], if we assume positive correlation between the damage dose (of γ-radiation, cytotoxic drugs) and the DNA damage (number of DSBs).

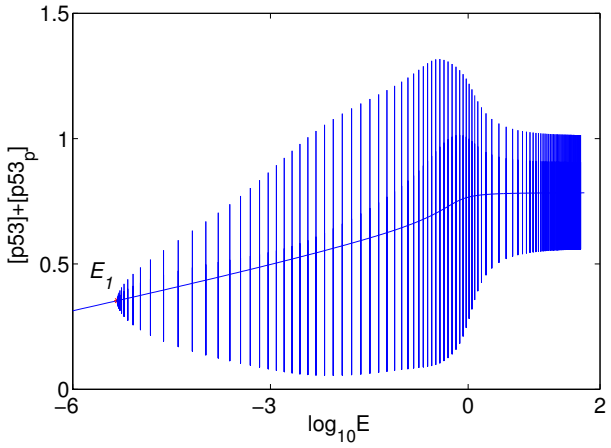

Figure 11: Bifurcation diagram for nuclear $[p53] + [p53_p]$ with respect to the varying signal E in the ODE system with the parameters in Table 2; E is in logarithmic scale. E_1 is the bifurcation point. Plotted curve for $E < E_1$ shows attained steady states and plotted bars for $E > E_1$ are the heights (showing maximum and minimum) of the amplitudes of stable limit cycles.

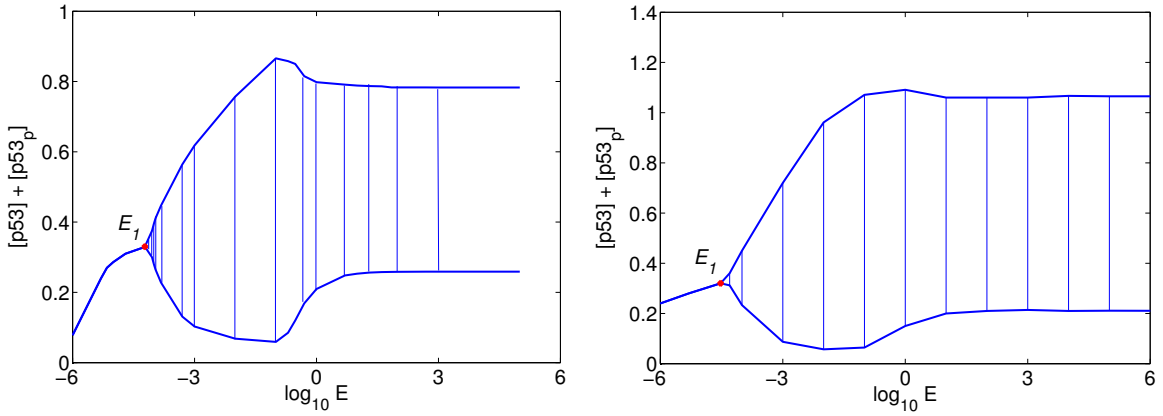

(a) (b)

Figure 12: Bifurcation diagram for nuclear $[p53] + [p53_p]$ with respect to the varying signal E, (a) in the 2D, (b) in the 3D PDE system with the parameters in Tables 2 and 5; E is in logarithmic scale. E_1 is the bifurcation point. Plotted curve for $E < E_1$ shows attained steady states and plotted bars for $E > E_1$ are the heights (showing maximum and minimum) of the amplitudes of stable limit cycles.

The amplitudes of oscillations should be independent of the damage dose as well; in our simulations, the amplitudes firstly increase for the values of E between E_1 and $\sim$0.1, then they slightly decrease and, for $E > 10$, the oscillations do not change in amplitude.

Diffusion values for oscillations	Description	Dim.
$0.01 \leq D_{2,6}$	$D_{0,1,3,5} = 1000, D_4 = 300$ fixed	2D
$2 : 0.6 \leq D_{0,1,3,5} : D_4$	ratio $D_{0,1,3,5} : D_4$ and $D_{2,6} = 1.8$ fixed	2D
$1 : 0.3 : 0.0018 \leq D_{0,1,3,5} : D_4 : D_{2,6}$	ratio $D_{0,1,3,5} : D_4 : D_{2,6}$ fixed	2D
$0.1 \leq D_{2,6}$	$D_{0,1,3,5} = 1000, D_4 = 300$ fixed	3D
$1 : 0.3 \leq D_{0,1,3,5} : D_4$	ratio $D_{0,1,3,5} : D_4$ and $D_{2,6} = 1.8$ fixed	3D
$5 : 1.5 : 0.009 \leq D_{0,1,3,5} : D_4 : D_{2,6}$	ratio $D_{0,1,3,5} : D_4 : D_{2,6}$ fixed	3D

Table 6: Ranges for the diffusion parameters (in $\mu m^2/min$) for which the 2D and 3D PDE systems give oscillations, assuming that the considered ratios and the unmentioned parameters from Tables 2 and 5 are fixed. As for the reference values, $D_{0,1,3,5} = 1000$, $D_4 = 300$ and $D_{2,6} = 1.8\,\mu m^2/min$ for the p53 (Mdm2, Wip1), ATM and mRNPs, respectively, have been taken. (Dim. stands for dimension.)

5.4. Parameter sensitivity analysis: diffusivity and permeability parameters

Once the oscillatory mode is established for the particular set of parameters, robustness of the PDE system to spatial perturbations can be examined, i.e. one can vary the spatial parameters, namely, diffusivity and permeability. The reference diffusion coefficients for proteins $D_{0,1,3,5} = 1000\,\mu m^2/min$, $D_4 = 300\,\mu m^2/min$ and for mRNPs $D_{2,6} = 1.8\,\mu m^2/min$ (Table 5) are partially obtained from experiments and can thus be considered as the realistic ones. On the other side, the reference permeabilities $p_{0,1,5} = 10\,\mu m/min$ and $p_{2,6} = 0.36\,\mu m/min$ (Table 5) have been chosen based on our simulations. Recall that $p53_p$ and ATM_p are assumed not to be transported from the nucleus and thus the permeabilities for these two proteins are taken to be zero, i.e. $p_{3,4} = 0\,\mu m/min$. The parameters from Table 2 are fixed in the sequel.

Let us now fix the reference permeability coefficients, i.e. let us assume that the nuclear membrane has its "carrying capacity" fixed and cargoes are allowed to be transported through the membrane in the same manner whatever cargo cytosol diffusivities are. For the fixed protein diffusivities (1000 and $300\,\mu m^2/min$), oscillations can be obtained for the diffusivity of mRNPs greater than 0.01 in 2D and $0.1\,\mu m^2/min$ in 3D simulations. Conversely, when the diffusivity rate for mRNPs is fixed to $1.8\,\mu m^2/min$, then the system exhibits oscillations for $D_{0,1,3,5} : D_4 \geq 2 : 0.6\,\mu m^2/min$ in 2D and for $D_{0,1,3,5} : D_4 \geq 1 : 0.3\,\mu m^2/min$ in 3D, respectively, whilst the ratio between the diffusivities for p53 (Mdm2, Wip1) and ATM is kept constant. Whenever the ratio between the proteins and mRNPs is kept fixed (equal to the ratio between the reference diffusivities), then oscillations appear for $D_{0,1,3,5} : D_4 : D_{2,6} \geq 1 : 0.3 : 0.0018\,\mu m^2/min$ in 2D and for $D_{0,1,3,5} : D_4 : D_{2,6} \geq 5 : 1.5 : 0.009\,\mu m^2/min$ in 3D simulations. Computed lower bounds for the diffusion rates are listed in Table 6. Interestingly, no upper bounds on the diffusivities are found where our simulations were executed for the diffusivities

Permeability values for oscillations	Description	Dim.
$0.05 \leq p_{2,6}$	$p_{0,1,5} = 10$ fixed	2D
$2 \leq p_{0,1,5}$	$p_{2,6} = 0.36$ fixed	2D
$1.5 : 0.054 \leq p_{0,1,5} : p_{2,6}$	ratio $p_{0,1,5} : p_{2,6}$ fixed	2D
$0.02 \leq p_{2,6}$	$p_{0,1,5} = 10$ fixed	3D
$1.5 \leq p_{0,1,5}$	$p_{2,6} = 0.36$ fixed	3D
$1.5 : 0.054 \leq p_{0,1,5} : p_{2,6}$	ratio $p_{0,1,5} : p_{2,6}$ fixed	3D

Table 7: Ranges for the permeability parameters (in $\mu m/min$) for which the 2D and 3D PDE systems give oscillations, assuming that the considered ratios and the unmentioned parameters from Tables 2 and 5 are fixed. As for the reference values, $p_{0,1,5} = 10$ and $p_{2,6} = 0.36\,\mu m/min$ for the p53 (Mdm2, Wip1) and mRNPs, respectively, have been taken. (Dim. stands for dimension.)

up to order 10^7. Higher diffusivities ($\sim 10^4\,\mu m^2/min$ and higher for the p53 protein) in any of the tested cases lead to oscillations with rather uniform shape, i.e., oscillations with constant amplitudes and periods.

Let us now fix the reference diffusion parameters and examine the PDE model with respect to the varying permeability rates. Firstly, let us fix the permeability for the proteins $p_{0,1,5} = 10\,\mu m/min$; then the oscillations appear for the mRNAs permeabilities $p_{2,6} \geq 0.05\,\mu m/min$ in 2D and $p_{2,6} \geq 0.02\,\mu m/min$, respectively. When $p_{2,6} = 0.36\,\mu m/min$ is fixed, then the system yields oscillations for $p_{0,1,5} \geq 2\,\mu m/min$ in 2D and for $p_{0,1,5} \geq 1.5\,\mu m/min$ in 3D simulations. Finally, if the ratio between the permeabilities for the proteins and mRNAs is constant (equal to the ratio between the reference permeabilities), then the oscillations can be attained for $p_{0,1,5} : p_{2,6} \geq 1.5 : 0.054\,\mu m/min$ in 2D and 3D. Again, no upper bounds have been detected. Computed ranges for the permeabilities which give a rise to oscillations are listed in Table 7.

Simulations thus show that the oscillations can be obtained for a broad range of spatial parameters.

5.5. The ER ensures robustness to spatial perturbations

So far, all the presented results assume the exclusion of synthesis from a ring-shaped "dead zone" around the nucleus (recalling that it has been proposed in [1, 45] that proteins able to enter the nucleus are not synthesized in the endoplasmic reticulum but only in free ribosomes in the cytoplasm, an assumption we endorsed in this PDE model). Importance of the ER immediately follows from complementary simulations where translation is permitted to occur in the ER, i.e. when the mRNA of Mdm2 and Wip1 can be translated into the proteins immediately after its translocation into the cytoplasm (in the areas B, C and D in Figure 5.), whilst p53 production is still assumed

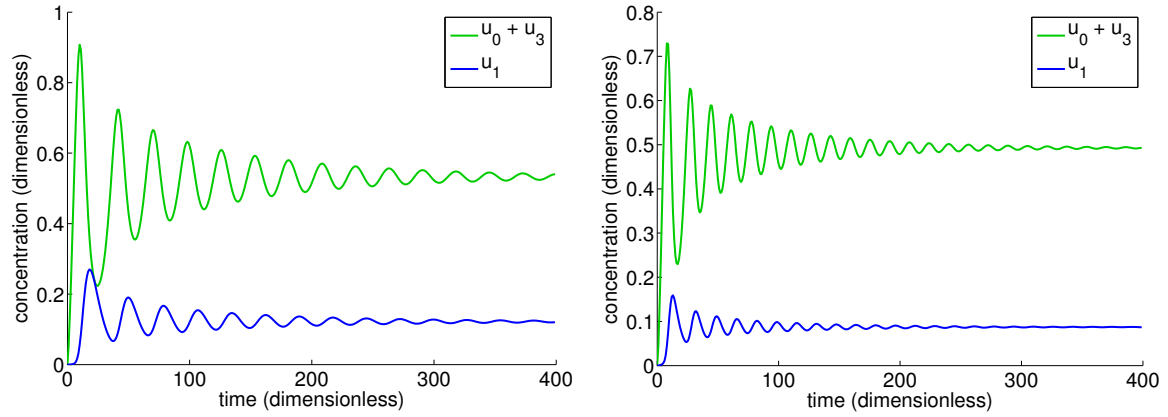

(a) $E = 10\,\mu M$ (b) $p_{2,6} = 10\,\mu m/min$

Figure 13: Solution of the 2D PDE system with translation of the proteins allowed in ER. Plots show the nuclear u_i and cytoplasmic v_i (dimensionless) concentrations of $p53 + p53_p$ ($u_0 + u_3$) and Mdm2 (u_2), (a) for $E = 10\,\mu M$ and (b) for $p_{2,6} = 10\,\mu m/min$. The remaining parameters in Tables 2 and 5 are unaltered. The plotted concentrations are the averages through all the elements of the nuclear and cytoplasmic triangulation, respectively.

to occur in a ring shaped area at distance from the nucleus (in the area C in Figure 5).

Figure 13 shows two plots of the nuclear p53 and ATM (dimensionless) concentrations where the activation signal has been increased from the reference value $E = 0.1\,\mu M$ to $10\,\mu M$, Figure 13(a), and where the permeability for the mRNAs has been increased from $p_{2,6} = 0.36\,\mu m/min$ to $10\,\mu m/min$, Figure 13(b) (while the other parameters in Tables 2 and 5 remain unchanged). The sustained concentrations in both subfigures disappeared. These results, when compared with the ranges for E and for the permeability for sustained oscillations in Table 7, suggest that sustained oscillations in cells with sharp or missing ER around the nucleus may not be obtained. While possible ranges for the diffusivities are not affected by omitting the ER, the permeabilities are bounded from above whenever the ER is excluded from the model.

5.6. Oscillations in cells of complicated structures

Besides the position of the ER which imposes additional delays into oscillations, thus making them more robust in the sense that oscillations can be retrieved for a broader range of the permeability coefficients, we further claim that oscillations can be obtained even in very complicated cell structures. As an example, a 2D Hela cell has been considered, Figure 14(a) and (b). The cell under consideration has an elliptic-like nucleus. The ER and an area for p53 basal production and mRNA translation have been chosen with the similar shape as the nucleus (not shown).

The PDE model (3) and (4) with the Kedem–Katchalsky boundary conditions (8) applied on the nuclear membrane and the zero flux boundary conditions (9) on the outer

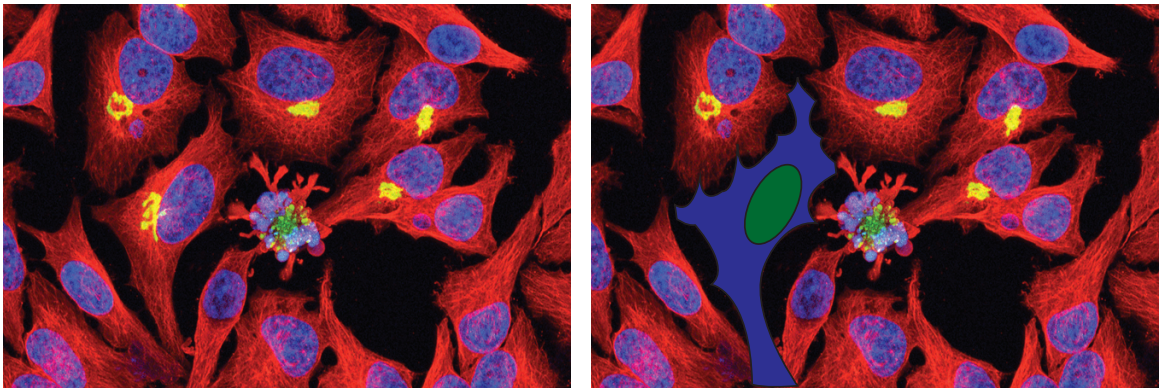

(a) (b)

Figure 14: (a) Healthy HeLa cells surrounding apoptotic HeLa cell (center). Image courtesy of Thomas Deerinck and Mark Ellisman (NCMIR and UCSD) [11]. Visible parts are the nucleus (blue), fibres (red) and Golgi's apparatus (yellow). (b) One particular cell chosen for simulations (nucleus is in green, cytoplasm in blue).

cellular membrane is then solved on the triangulation generated by FreeFem++. The kinetic rates, diffusion and translocation parameters remain the same as in Tables 2 and 5. The semi-implicit Rothe method [15] then gives oscillations in the p53 dynamics following exposition to a stress signal of the same amount of $E = 0.1$, see Figures 15(a) and (b) where the nuclear and cytoplasmic (dimensionless) concentrations of the proteins are plotted, Figures 15(c) and (d) for two particular phase planes that confirm existence of stable limit cycles in the protein evolutions, and also Figures 16 and 17 where six different samples from the concentrations of p53 and Mdm2 are captured. Time variable can be also rescaled by $\tau = 9.5$ so that the period of oscillations is again $\sim$6 hours.

6. Discussion

Based on the recently observed oscillations of the p53 protein in single cells [4, 20, 29], we proposed in [14] a physiological ODE model taking into account the negative feedback p53–Mdm2 together with ATM–p53–Wip1 which is reported as an integral part in retrieving p53 oscillations [4]. Unlike most of the existing p53 models, the oscillatory responses in our models are obtained with no additional positive feedback but rather by the compartmental distinction of cellular events between the nucleus and the cytoplasm.

In this paper we have embedded the ODE model [14] into a reaction–diffusion PDE model by introducing diffusivity in the protein signalling network. We have shown that spatial variables and the PDE model can be used to simulate the behaviour of the p53 intracellular network in the stressed cells as well. The oscillations obtained from PDEs have slightly smaller amplitudes and also different periods (which can still be rescaled to the observed p53 period of approximately 6 hours [4, 20]). This is caused by the actual spatial representation of the cell in the PDE settings, since in the PDE

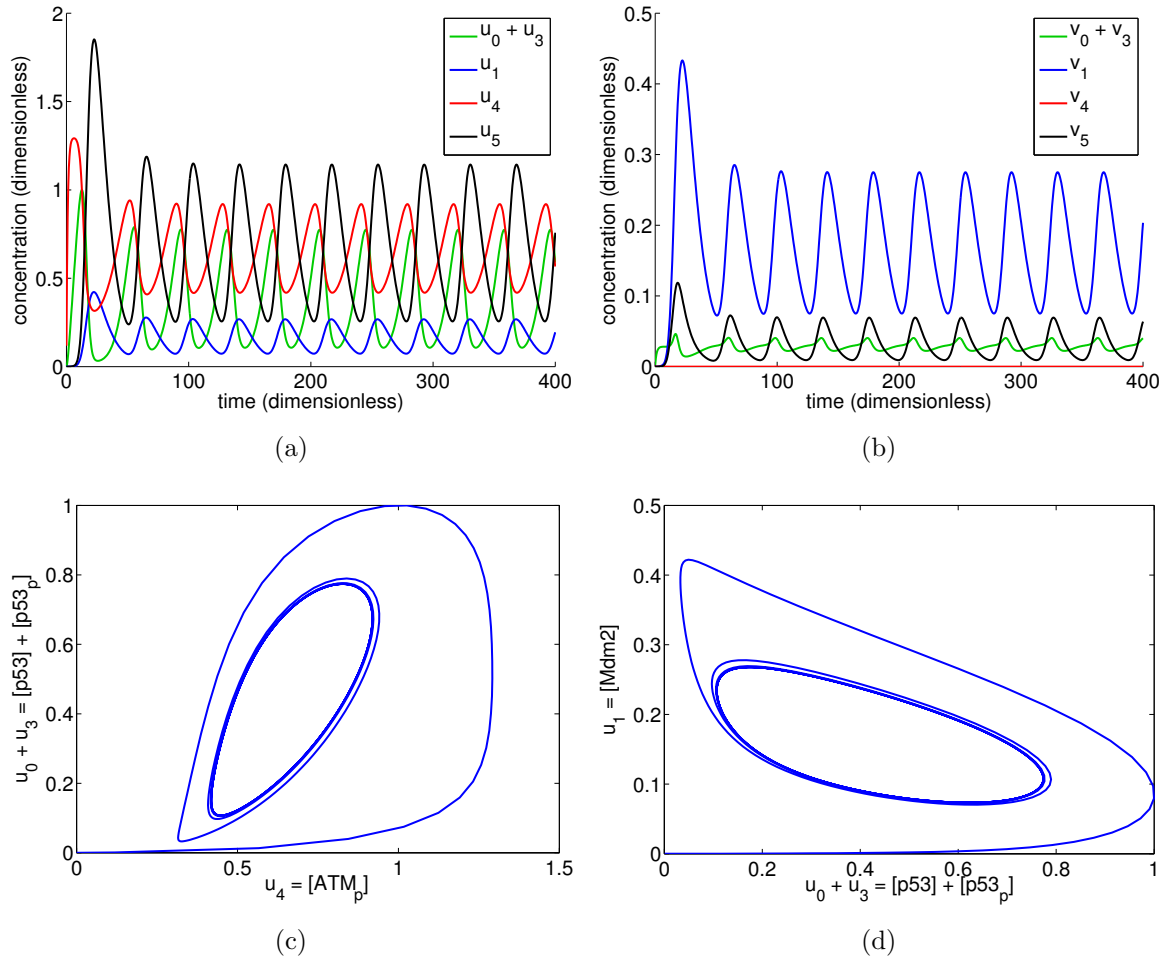

Figure 15: Solution of the 2D system on the HeLa cell: nondimensionalised (a) nuclear u_i and (b) cytoplasmic v_i concentrations of $p53 + p53_p$ ($u_0 + u_3$ and $v_0 + v_3$), $Mdm2$ (u_1 and v_1), ATM_p (u_4 and v_4), and $Wip1$ (u_5 and v_5). The plotted concentrations are the averages through the all elements of the nuclear and cytoplasmic triangulation. (c) phase portrait of $[ATM]$ with respect to $[p53]+[p53_p]$ (d) phase portrait of $[p53]+[p53_p]$ with respect to $[Mdm2]$.

model the species have to overcome distances diffusively to reach targets and particular areas in the cell, e.g. to reach the translations sites for mRNAs to be translated into proteins, which is not the case of ODEs. Translocation through the nuclear membrane, which is modelled by the Kedem–Katchalsky BCs, is also affected by diffusivity of the species. For example, Mdm2, which acts only in the nucleus, diffusively spreads over the entire cytoplasm after leaving the translation sites, which decreases its abundance at the nuclear membrane and so the level of the protein at the membrane that can be potentially translocated into the nucleus. Diffusive motion thus imposes a delay in the Mdm2 protein translocation into the nucleus which, afterwards, affects the amplitudes and period of its concentration. Translocation in ODEs is simplified in the way that

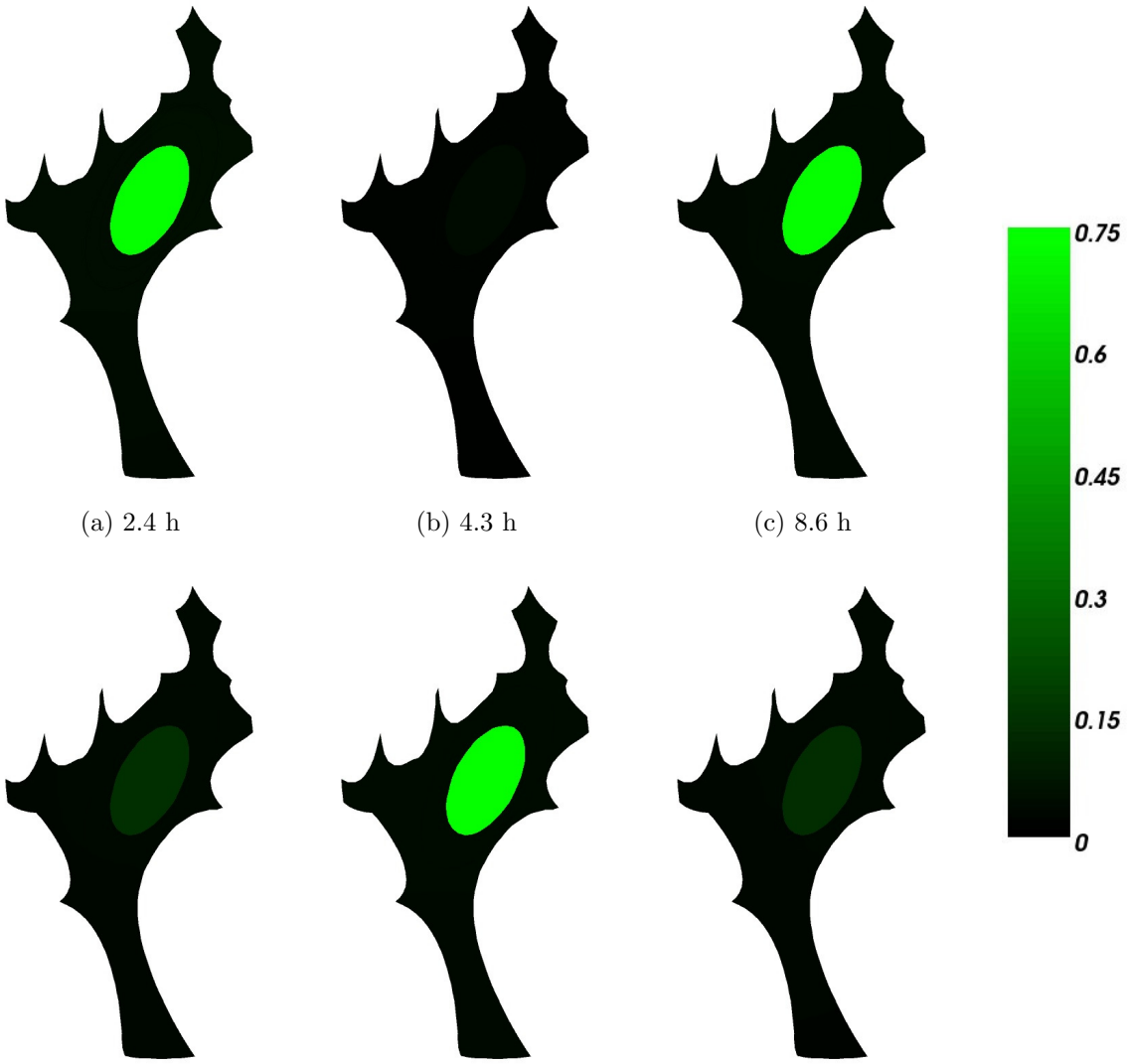

(a) 2.4 h (b) 4.3 h (c) 8.6 h

(d) 10.5 h (e) 14.7 h (f) 16.6 h

Figure 16: 2D visualisation of the solution of the PDE system for the HeLa cell: nondimensionalised concentration of $p53_p$ and $p53$. Chosen samples are captured at times (scaled by $\tau = 9.5$) when p53 and Mdm2 reach peaks in concentration.

the actual concentrations at the nuclear membrane are the concentrations in the whole compartments thus independent of the effect of diffusive movement. Hence, diffusivity, the time the species need to reach membranes, compartments and the translation zones within the cytoplasm, translocation through the nuclear membrane (controlled by the permeability of the membrane), *etc.*, regulate p53 dynamics by imposing sufficient physiological delays, resulting in sustained oscillations.

Note that the exclusion of synthesis, for the proteins under study, from the endoplasmic reticulum, as it has been proposed in [1, 45], endows the PDE system with additional delays for regulation without changing the ODE parameter set. Figure 13

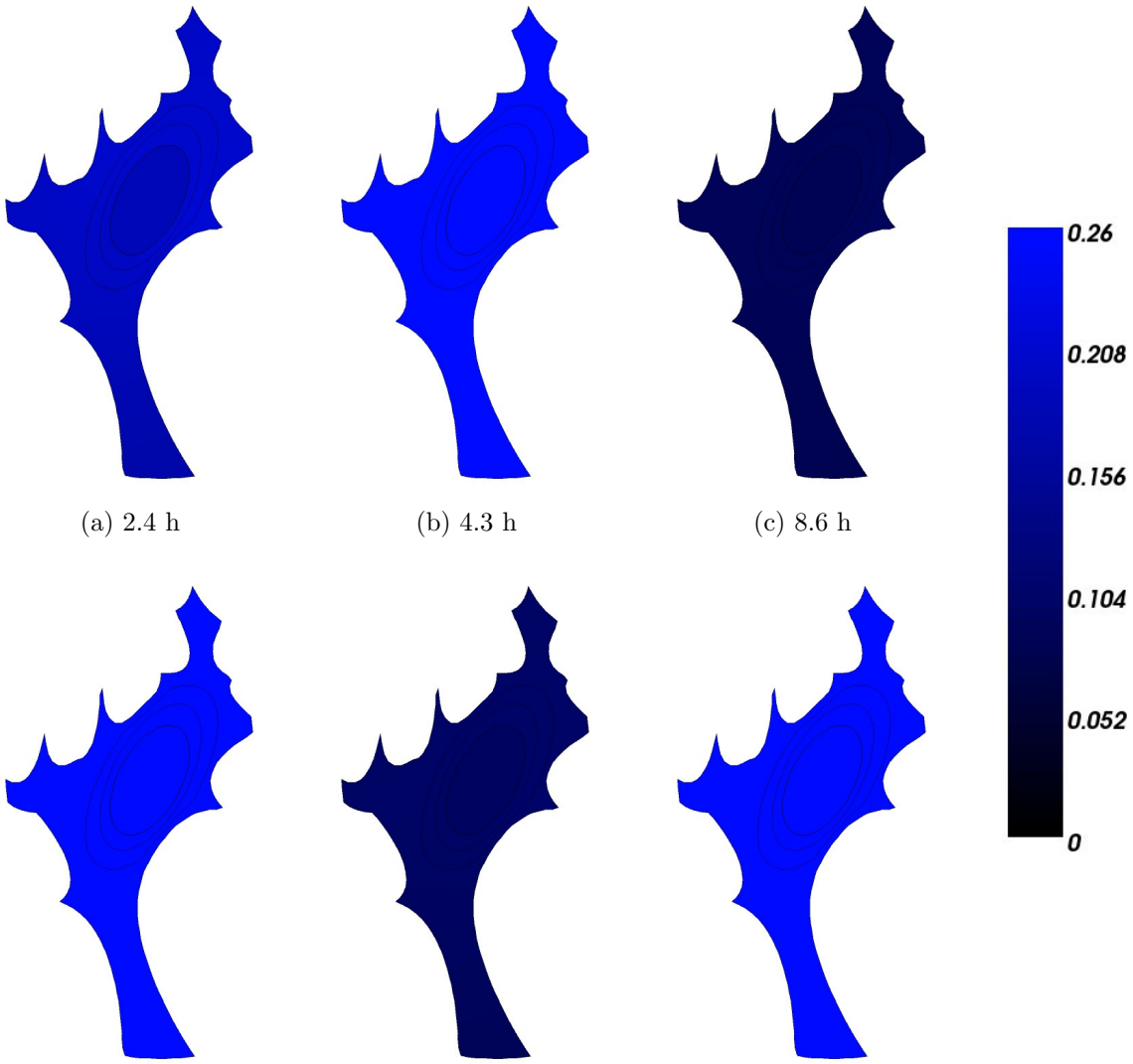

(a) 2.4 h (b) 4.3 h (c) 8.6 h

(d) 10.5 h (e) 14.7 h (f) 16.6 h

Figure 17: 2D visualisation of the solution of the PDE system for the HeLa cell: nondimensionalised concentration of $Mdm2$. Chosen samples are captured at times (scaled by $\tau = 9.5$) when p53 and Mdm2 reach peaks in concentration.

shows examples where, for example, the 2D PDE system with the permeability for the mRNAs increased from the reference value $0.36\,\mu m/min$ to $10\,\mu m/min$ (the reference value for the protein permeability) does not show sustained oscillations. In [13], the authors also use the same kinetic rates for both ODE and PDE system, and still obtain oscillations, however, with different diffusion and permeability coefficients. The diffusion rates chosen here ($\sim 1000 \mu m^2/min$ for p53, Mdm2 and Wip1) lie at the upper bound of the estimated range of acceptable diffusion coefficients for p53 and Mdm2 for which simulations in [13] yield oscillations. The estimated range of the diffusion parameters, for which our PDE system gives oscillations, is rather wide (even with no upper bounds

in 2D and 3D simulations, Table 6) compared with the range $10 - 1000\,\mu m^2/min$ for the protein diffusivity obtained in [13] and the range $4.44 - 150\,\mu m^2/min$ given by the PDE model in [45] for the diffusivities of both proteins and mRNAs.

Sustained oscillations can be reproduced in cells with complicated morphologies as in those in Figure 14, however, with some restrictions on the permeability of the nuclear membrane. These restriction can be partially abolished by the inclusion of the well defined ER, although the ER does not necessarily have to present smooth boundaries. Hence, the ER around the nucleus sets limits on the range of acceptable permeabilities needed for oscillations; the narrower the ER is, the smaller range of permeabilities for oscillations exists.

Unlike with the chosen set of parameters in the ODE model in [14], in the ODE model presented here we have slightly changed some rates, in particular, unknown parameters in the expression of Wip1 by p53 so that Wip1 and Mdm2 transcription by p53 runs with no affinity of p53 for these target genes. These modifications do not alter dynamical responses of the system. However, bearing in mind the expected behaviour of p53, i.e. turning off its oscillations in some point and establishing a steady state of high levels signalising started apoptosis, we chose in [14] the reference concentrations for the proteins in nondimensionalisation without deeper consideration so that the ODE system has two Hopf bifurcation points signalising two qualitatively different states for the damage signal E, the main bifurcation parameter under consideration (see Section 3.6 for the introduction of E). Indeed, a bifurcation analysis of the ODE system in [14] with respect to E reveals two supercritical Hopf bifurcation points in the equilibrium curve starting at $E = 0$. In [14] the equilibrium changed from stable to unstable by passing through the first Hopf point E_1 and then back from being unstable to stable when E crosses the second Hopf point E_2. This means that the solution bifurcates between two qualitatively different states: convergence to a steady state for $E < E_1$ and $E > E_2$, and convergence to a stable limit cycle for $E_1 < E < E_2$.

We speculated in [14] that these Hopf points E_1 and E_2 may represent in a very summarised form key points in the p53-mediated cell fate decisions. In particular, whenever p53 oscillatory signalling is necessary for DNA repair, the damaged DNA signal E is produced so that $E_1 < E < E_2$. For these values of E, p53 sustainedly oscillates with a possible physiological interpretation of the oscillations as a periodical examination of persistence of DNA DSBs as proposed in [4, 29]. If the number of DSBs decreases in repair processes and p53 oscillations are not needed anymore, then also E might decrease, and become potentially smaller than E_1 or completely extinct if the DNA damage is successfully fixed. Therefore, E might turn off the oscillations of the proteins. This speculation can be partially supported by some experiments, for example, it has been reported in [3] that transient and temporal DNA DSBs (as the occasional ones occurring in DNA synthesis) do not result in ATM and p53 oscillations, and these occasional DSBs may be related to $E < E_1$. However, if DSBs persist, even more when their number increases, and/or it is impossible to repair them, then the cell might decide to launch apoptosis with amplified E so that E trespasses the threshold

E_2. In apoptotic cells then the concentration of p53 leaves oscillations and approaches its steady state of high values, for example, due to the compartmental regulation of the proteins in the p53 pathway, as an Akt-dependent inhibition of Mdm2 translocation into the nucleus in such cells [7, 21].

The activation signal E is understood in [14], similarly as it is understood in this paper, as the measure of the DNA damage, and we assume that it is positively correlated with the damage doses (the higher doses a cell is exposed to, the bigger number of DSBs is caused, the stronger activation signal E is produced; although closer identification of E with the number of DSBs is not resolved in our works). Experiments on the p53 signalling network in single cells show that the oscillations can be observed independently of the damage dose and that the probability for starting pulsatile response becomes greater with the increasing number of DSBs [20, 35]. Thus, based on such strong evidence, the oscillations of the system should not become extinct with increasing E as it was modelled by the ODE model in [14] provided that E corresponds to the damage dose. The signal E in [14] apparently plays a stronger role in the p53 signalling since it can turn off the oscillations by itself. However, further studies need to be done to somehow give a biological basis to our abstract parameter E and either accept or reject our speculations.

The ODE and PDE systems presented in this paper and the ODE model in [14] exhibit a supercritical Hopf point starting from which, when E increases, the solution maintains sustained oscillations instead of converging to a steady state. This bifurcation point can have a biological explanation as above. However, the second point for which sustained oscillations are switched back into the convergence to a steady state by crossing this point does not appear anymore in the present study as illustrated on Figures 11 and 12. Thus, as it has been reported in [20, 29], p53 oscillations can be modelled as a response of the cell to stress agents independently of the abundance of such agents, i.e. the oscillations are not turned off just by considering increased DNA damage.

Apoptosis of the cell can still be accompanied by the concentration of p53 switched from the oscillatory response to the DNA damage to a stable steady state of high levels. Note that the p53 sustained oscillations observed in [4, 20, 29], which can persist as long as 3 days (and possibly longer), have been demonstrated in breast cancer cells MCF-7 lacking functional PTEN protein, thus, indeed, the p53-PTEN-PIP3-Akt positive feedback may play an essential role in cell fate decisions [7, 21]. The compartmental ODE models [38, 53] consider effects of this particular positive feedback. It is, for example, proposed in [38] that the p53-PTEN-PIP3-Akt positive feedback works as a clock behind the p53-Mdm2 negative feedback, which gives some time ($\sim$15 hours) to repairing processes to fix the DNA damage, otherwise, irreversible apoptosis is launched. In addition, the p53-Mdm2 negative feedback alone is used to gain sustained oscillations in [38], however, it has been shown inefficient to produce oscillations in vivo [4]. The ODE model in [53] consists of the two negative feedbacks as they are considered in our models. A cell fate decision is determined by one of the two different p53 states, p53-arrester and p53-killer, the latter overcoming the former. The p53-arrester firstly

transcribes pro-arrest genes (Wip1, p53DINP1 and p21) and subsequently blocks the cell cycle, while p53-killer transcribes pro-apoptotic genes (PTEN, p53DINP1 and p53AIP1) later on, thus directing the cell to death. Note that this concept is based on the affinity of p53 for the target genes that contradicts recently published observations in [28].

The aim of this work, rather simple compared with the overall complexity of p53 signalling network in cell fate decisions between survival and death, is to simulate activation of p53 in single cells which concentration is led to sustained oscillations under stress conditions, the duration of oscillations being independent of the damage signal. Thus, we simplified the p53 network by neglecting (hundreds of) possible target proteins and kept only those proteins that are actually experimentally justified to be necessary and sufficient for oscillations. Thus, four proteins, particularly, p53, Mdm2, Wip1 and ATM have been chosen [4], and the ODE and reaction-diffusion PDE models were proposed for this purpose. Plausible effects of any positive feedback are not disputed in our work.

7. Conclusions

At this step of modelling we have represented and simulated p53 immediate responses to various stress conditions disrupting the integrity of the genome, such as γ-radiation or drugs in chemotherapies causing DNA DSBs. In such cases, the DNA damage sensor ATM activates p53, thus endowing it with the ability to subsequently act as a transcription factor. Such responses to stress agents can be very sensitive in mammalian cells and our models also show sensitivity in producing oscillatory responses for very low values of the damage signal, E. On the other side, the duration of the oscillatory response is not terminated purely by increasing E. Including p53-mediated cell decisions between survival and death into the models is naturally the next step in our modelling work, which will be tackled in papers to follow. We stress again here, as already stated in [14], that the aim we pursue is to elicit the mechanisms involving p53 that lead a cell with damaged DNA to cell cycle arrest, apoptosis or repair. Intracellular spatial models, based on minimal physiologically identified mechanisms, and involving reaction–diffusion equations, are to our meaning the most natural tool towards this goal.

References

[1] Alberts B, *et al* 2008 *Molecular Biology of the Cell. Garland Science* fifth ed. (Taylor and Francis Group Ltd, Oxford).

[2] Bakkenist J Ch and Kastan M B 2003 DNA damage activates ATM through intermolecular autophosphorylation and dimer dissociation, Nature **421**, 499–506.

[3] Bartkova J, *et al* 2005 ATM activation in normal human tissues and testicular cancer, Cell Cycle **4**, 838–845.

[4] Batchelor E, *et al* 2008 Recurrent Initiation: A mechanism for triggering p53 pulses in response to DNA damage, Molecular Cell **30**, 277–289.

[5] Braga J, McNally J G and Carmo-Fonseca M 2007 A Reaction-Diffusion Model to Study RNA Motion by Quantitative Fluorescence Recovery after Photobleaching, Biophysical Journal **92**, 2694–2703.

[6] Cangiani A and Natalini R 2010 A spatial model of cellular molecular trafficking including active transport along microtubules, J. Theor. Biol. **267**, 614–625.

[7] Cantley L C and Neel B G 1999 New insight into timor suppression: PTEN suppresses timor formation by restraining the phosphoinositide 3-kinase/AKT pathway, Proc. Natl. Acad. Sci. USA **96**, 4240–4245.

[8] Ciliberto A, Novak B and Tyson J J 2005 Steady states and oscillations in the p53/Mdm2 network, Cell Cycle **4**, 488–493.

[9] Clairambault J 2009 Modelling physiological and pharmacological control on cell proliferation to optimise cancer treatments, Mathematical Modelling of Natural Phenomena **4**, 12–67.

[10] Cole C N and Scarcelli J J 2006 Transport of messenger RNA from the nucleus to the cytoplasm, Current Opinion in Cell Biology **18**, 299–306.

[11] Deerinck T and Ellisman M 2008 Death Most Beautiful (Photograph), from http://www.cell.com/cell_picture_show-celldeath.

[12] DeFranco C, Chicurel M E and Potter H 1998 A General RNA-Binding Protein Complex That Includes the Cytoskeleton-associated Protein MAP 1A, Mol Biol Cell **9**(7), 1695–1708.

[13] Dimitrio L, Clairambault J and Natalini R 2013 A spatial physiological model for p53 intracellular dynamics, Journal of Theoretical Biology **316**, 9–24.

[14] Eliaš J, Dimitrio L, Clairambault J and Natalini R 2014 The p53 protein and its molecular network: dynamic modelling of a missing link between the effects of anticancer cytotoxic drugs on DNA damage and cell proliferation in healthy and cancer cell populations, Biochimica et Biophysica Acta (BBA Proteins and Proteomics) **1844**, 232–247.

[15] Eliaš J and Clairambault J 2014 Reaction-diffusion systems for spatio-temporal intracellular protein networks: a beginner's guide with two examples. Submitted.

[16] Falck J, Coates J and Jackson S P 2005 Conserved modes of recruitment of ATM, ATR and DNA-PKcs to sites of DNA damage, Nature **434**, 605–6011.

[17] Fiscella M, *et al* 1997 Wip1, a novel human protein phosphatase that is induced in response to ionizing radiation in a p53-dependent manner, Proc. Natl. Acad. Sci. USA **94**, 6048–6053.

[18] FreeFem++, an open source, high level integrated developmental environment for numerical solving partial differential equations, available at http://www.freefem.org/++/.

[19] Friedman P N, *et al* 1993 The p53 protein is an unusually shaped tetramer that binds directly to DNA, Proc. Natl. Acad. Sci. USA **90**, 3319–3323.

[20] Geva-Zatorsky N, *et al* 2006 Oscillations and variability in the p53 system, Molecular Systems Biology **2**, 1–13.

[21] Gottlieb T M, *et al* 2002 Cross-talk between Akt, p53 and Mdm2: possible implications for the regulation of apoptosis, Oncogene **21**, 1299–1303.

[22] Harris S L and Levine A J 2005 The p53 pathway: positive and negative feedback loops, Oncogene **24**, 2899–2908.

[23] Hinow P, *et al* 2006 The DNA Binding Activity of p53 Displays Reaction-Diffusion Kinetics,

Biophysical Journal **91**, 330–342.
[24] Hong S, *et al* 2010 MEASUREMENT of Protein 53 Diffusion Coefficient in Live HeLa Cells Using Raster Image Correlation Spectroscopy (RICS), Journal of Biomaterials and Nanobiotechnology **1**, 31–36.
[25] Joerger AC and Fersht AR 2010 The Tumor Suppressor p53: From Structures to Drug Discovery, Cold Spring Harb Perspect Biol **2:a000919**.
[26] Keener J P and Sneyd J 2009 *Mathematical Physiology I: Cellular Physiology* second ed. (Springer).
[27] Kim J K and Jackson T L 2013 Mechanisms That Enhance Sustainability of p53 Pulses, PLoS ONE 8(6): e65242. **doi:10.1371/journal.pone.0065242**.
[28] M. Kracikova, *et al* 2013 A threshold mechanism mediates p53 cell fate decision between growth arrest and apoptosis, Cell Death & Differentiation **20**, 576–588..
[29] Lahav G, *et al* 2004 Dynamics of the p53-Mdm2 feedback loop in individual cells, Nature Genetics **36**, 147–150.
[30] Lain S and Lane D 2003 Improving cancer therapy by non-genotoxic activation of p53, European Journal of Cancer **39**, 1053–1060.
[31] Lee J H and Paull T T 2005 ATM activation by DNA double-strand breaks through the Mre11-Rad50-Nbs1 complex, Science **308**, 551–554.
[32] Levine A J 2011 The paths to death and differentiation, Cell Death and Differentiation **18**, 1391–1392.
[33] Li M, *et al* 2003 Mono- Versus Polyubiquitination: Differential Control of p53 Fate by Mdm2, Science **302**, 1972–1975.
[34] Link D C, *et al* 2011 Identification of a Novel TP53 Cancer Susceptibility Mutation Through Whole-Genome Sequencing of a Patient With Therapy-Related AML, JAMA **305**:15, 1568–1576.
[35] Loewer A, *et al* 2013 The p53 response in single cells is linearly correlated to the number of DNA breaks without a distinct threshold, BMC Biology **11**:114, 13 pages.
[36] Ma L, *et al* 2005 A plausible model for the digital response of p53 to DNA damage, Proc. Natl. Acad. Sci. USA **102**, 14266–14271.
[37] Nagy E 2012 *Basic Equations of the Mass Transport through a Membrane Layer* first ed. (Elsevier, Amsterdam).
[38] Puszyński K, Hat B and Lipniacki T 2008 Oscillations and bistability in the stochastic model of p53 regulation, Journal of Theoretical Biology **254**:2, 452–465.
[39] Ribbeck K and Görlich D 2001 Kinetic analysis of translocation through nuclear pore complexes, The EMBO Journal **20**:6, 1320–1330.
[40] Roubíček T 2013 *Nonlinear Partial Differential Equations with Application* second ed., Chapter 8, (Springer, Basel).
[41] Segel L A 1972 Simplification and scaling, SIAM Rev. **14**, 547–571.
[42] Shreeram S, *et al* 2006 Wip1 Phosphatase Modulates ATM-Dependent Signaling Pathways, Molecular Cell **23**, 757–764.
[43] Shreeram S, *et al* 2006 Regulation of ATM/p53-dependent suppression of myc-induced lymphomas by Wip1 phosphatase, The Journal of Experimental Medicine **203**, 2793–2799.
[44] Stommel J M, *et al* 1999 A leucine-rich nuclear export signal in the p53 tetramerization domain: regulation of subcellular localization and p53 activity by NES masking, The EMBO Journal **18**:6, 1660–1672.
[45] Sturrock M, *et al* 2011 Spatio–temporal modelling of the Hes1 and p53-Mdm2 intracellular signalling pathways, Journal of Theoretical Biology **273**, 15–31.
[46] Vargas D Y, *et al* 2005 Mechanism of mRNA transport in the nucleus, PNAS **102**, 17008–17013.
[47] Vogelstein B, Lane D and Levine A J 2000 Surfing the p53 network, Nature **408**, 307–310.
[48] Vousden K H and Lane D P 2007 p53 in health and disease, Nature Reviews Molecular Cell Biology **8**, 275–283.
[49] Wagner J, *et al* 2005 p53–Mdm2 loop controlled by a balance of its feedback strength and effective

dampening using ATM and delayed feedback, Proc. Natl. Acad. Sci. USA **102**, 109–118.

[50] Weinberg R L, Veprintsev D B and Fersht A R 2004 Cooperative binding of tetrameric p53 to DNA, J. Mol. Biol **341**, 1145–1159.

[51] Young D B, *et al* 2005 Identification of Domains of Ataxia-telangiectasia Mutated Required for Nuclear Localization and Chromatin Association, The Journal of Biological Chemistry **280**, 27587–27594.

[52] Zhang T, Brazhnik P and Tyson J J 2007 Exploring mechanisms of the DNA-damage response: p53 pulses and their possible relevance to apoptosis, Cell Cycle **6**, 85–94.

[53] Zhang X P, Liu F and Wang W 2011 Two-phase dynamics of p53 in the DNA damage response, Proc. Natl. Acad. Sci. USA **22**, 8990–8995.

[54] Zhao Z, *et al* 2010 p53 loss promotes acute myeloid leukemia by enabling aberrant self-renewal, Genes Dev **24**, 1389–1402.

[55] Murray-Zmijewski F, Slee E A and Lu X 2008 A complex barcode underlies the heterogeneous response of p53 to stress, Nature, Rev. Mol. Cell Biol. **9**, 702–712.